공학석사학위논문

All-speed Two-phase Computations for General Equation of State with Preconditioning Techniques and Scaling of Numerical Dissipations

예조건화 기법과 수치점성 조절을 통한 전마하수 이상유동 계산

2015 년 2 월

서울대학교 대학원

기계항공공학부

김 현 지

All-speed Two-phase Computations for General Equation of State with Preconditioning Techniques and Scaling of Numerical Dissipations

예조건화 기법과 수치점성 조절을 통한 전마하수 이상유동 계산

지도교수 김 종 암

이 논문을 공학석사 학위논문으로 제출함

2015 년 2 월

서울대학교 대학원

기계항공공학부

김 현 지

김현지의 공학석사 학위논문을 인준함

2015 년 2 월

위 원 장	김 규 홍	(인)
부위원장	김 종 암	(인)
위 원	이 관 중	(인)

Abstract

The present research focuses on the system preconditioning and the scaling of numerical dissipations of RoeM and AUSMPW+ methods to enable more efficient and accurate computations of all-speed two-phase flows. Previous all-speed two-phase RoeM and AUSMPW+ methods have applied only steady system preconditioning technique while unsteady system preconditioning is essential for the convergence acceleration of unsteady low Mach number flows. In this study, unsteady system preconditioning is achieved by the consideration of Strouhal number in preconditioning parameter. Unlike existing preconditioning techniques, scaling factors in numerical dissipations are treated separately with preconditioning parameter in system so that the numerical instability and the accuracy degradation issues in low Mach number regions are resolved regardless of the convergence. The extension of two-phase RoeM and AUSMPW+ methods to general equation of state (EOS) is completed through the modification of shock discontinuity sensing term (SDST) to be independent on EOS. The performance of the modified SDST is confirmed to be as stable as the previous SDST which works well, but is compatible only with specific forms of EOS.

Keywords: All-speed flow, Two-phase flow computation, Preconditioning, Scaling of numerical dissipations, Shock discontinuity sensing term (SDST), Homogeneous mixture model

Student Number: 2013-20665

Contents

List of Figures

List of Tables

Chapter 1

Introduction

1.1 Computation of All-speed Two-phase Flows

The analysis of two-phase flows has become one of the definite currents in CFD field. Of course, enormous examples of two-phase flows in nature and corresponding numerous applications in engineering have been powerful motivations of this progress. Such examples are combustion, cavitation, steam generation and condensation in nuclear reactor, explosion in water, liquid shock and gas bubble interaction, and so on. With the aid of increase in computing power, even massive 3D two-phase computations are now possible and utilized as an indispensable tool for various engineering problems. Nevertheless, many numerical issues in this area are waiting to be resolved for more efficient and accurate computations.

One of the important issues is about equation of state (EOS). The scope of two-phase problems analyzed by CFD at the moment is mostly limited to the case of frequently used fluids such as water and air. In other words, most

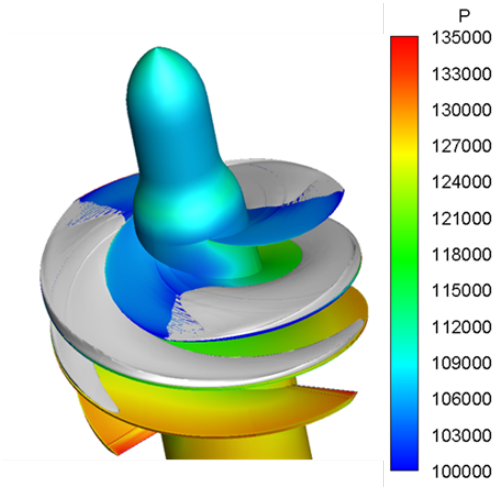

Figure 1.1: Cryogenic cavitation around turbopump inducer

problems can be treated with a few EOSs like ideal gas law or stiffened EOS. However, several EOSs cannot cover all types of working fluids and operting conditions like water at extreme environment, cryogens(LH_2, LO_2, LN_2), liquid fuels(gasoline, kerosene, LPG, ammonia), etc. Considering various working fluids under diverse operating conditions in academia and industries, two-phase computations need to be extended to encompass these wide range of EOSs. If numerical methods we use have dependency on certain EOS, the situation becomes problematic when dealing with other fluids of different form of EOS.

Another issue in two-phase flow computations is preconditioning. Figure 1.1 [1] shows cryogenic cavitation which should be computed by compressible solver because of the thermal effects of cryogens. However, coexistence of compressible and incompressible flow fields requires our numerical methods to handle not only compressible flows but all-speed flows from very low Mach number to supersonic flow with shock waves. Likewise, many examples of two-phase flows innately have both compressible and incompressible flow regions. They need

to be computed by all-speed numerical methods, since in two-phase flows, one phase can be considered almost incompressible in comparison with the other phase and this circumstance often makes the compressible solver give disastrous solution or worse, fail to converge. Proper preconditioning to compressible system improves convergence, but it yields unwanted stability problem in low Mach number limit.

1.2 Thesis Objectives

Keeping the issues of EOS and preconditioning in mind, we need to examine the precedent studies on all-speed two-phase computations and preconditioning techniques. For all-speed two-phase computations, RoeM and AUSMPW+ methods in gas dynamics which are known as accurate and efficient shock-stable schemes have been extended to two-phase versions [2]. The extended methods are also robust and efficient for compressible two-phase flows and they can deal with compressible-incompressible two-phase flows with application of steady preconditioning technique. Despite these strengths, two schemes are limited to two-phase flows of water and ideal gas only since they contain a term which is dependent on specific forms of EOSs. Also, they are not able to compute unsteady low Mach number flows accurately as unsteady system preconditioning and proper scaling of numerical dissipations are not considered.

For unsteady system preconditioning, consideration of Strouhal number in preconditioning process was found to result in convergence acceleration for unsteady low Mach number flows and optimal scaling required for spatial accuracy was concerned as well [3], [4], [5], [6]. Separate study on the scaling of numerical dissipations independent with the system preconditioning was also carried out for Roe-type schemes [7]. This paper pays attention to the order of each term

in numerical dissipations to avoid non-physical behavior, global cut-off problem and checkerboard instability appeared in the low Mach number limit.

The objective of the present work is to extend the previous all-speed two-phase RoeM and AUSMPW+ methods to general EOS with the application of unsteady system preconditioning through Strouhal number. While applying steady/unsteady system preconditioning, numerical dissipations are to be scaled separately unlike existing preconditioning methods to avoid accuracy degradation problem and numerical instability in the low Mach number flows.

The present work is organized as follows. After introduction, a brief description of the governing equation and conventional (steady) system preconditioning technique is given. In Chapter 3, extension of two-phase RoeM and AUSMPW+ methods to general EOS is described by modification of shock discontinuity sensing term (SDST), followed by unsteady preconditioning and scaling of numerical dissipations. Various test cases are carried out to validate newly designed SDST and the proposed preconditioning and scaling methods. Finally, conclusions are drawn in Chapter 5.

Chapter 2

Governing Equations

2.1 Homogeneous Mixture Equations

2.1.1 Two-phase Navier-Stokes Equations

The homogeneous mixture equations are adopted to describe two-phase flows. Here, the mixture of two different phases is assumed as a pseudo-fluid whose pressure, velocity and temperature are determined by suitable averages of the properties of constituent phases. Underneath this assumption lies a view that it is sufficient to describe each phase, including pseudo-fluid as well as pure liquid and gas phase, as a macroscopic continuum obtained from appropriate averaging process. Since the pseudo-fluid is not an equilibrium state of liquid and gas phases, one phase mass-conservation law is additionally needed to account for the phase change. Therefore, the governing equations consist of mixture mass-, momentum-, energy-conservation laws, together with one phase

mass-conservation law as follows:

$$\frac{\partial \mathbf{Q}}{\partial t} + \nabla \cdot (\mathbf{F} - \mathbf{G}) = \mathbf{S}_{phasechage}, \tag{2.1}$$

where $\mathbf{Q}$ is the conservative variable vector defined by

$$\mathbf{Q} = \left[\begin{array}{ccccccc} \rho_m & \rho_m u & \rho_m v & \rho_m w & \rho_m E_t & \rho_m Y_1 \end{array} \right]^T. \tag{2.2}$$

$\mathbf{F}$ and $\mathbf{G}$ indicate the inviscid flux tensor and the viscous flux tensor. For three-dimensional case,

$$\mathbf{F} = \left[\begin{array}{ccc} \rho_m u & \rho_m v & \rho_m w \\ \rho_m u^2 + p & \rho_m uv & \rho_m uw \\ \rho_m vu & \rho_m v^2 + p & \rho_m vw \\ \rho_m wu & \rho_m wv & \rho_m w^2 + p \\ \rho_m uH & \rho_m vH & \rho_m wH \\ \rho_m uY_1 & \rho_m vY_1 & \rho_m wY_1 \end{array} \right], \ \mathbf{G} = \left[\begin{array}{ccc} 0 & 0 & 0 \\ \tau_{xx} & \tau_{yx} & \tau_{zx} \\ \tau_{xy} & \tau_{yy} & \tau_{zy} \\ \tau_{xz} & \tau_{yz} & \tau_{zz} \\ \theta_x & \theta_y & \theta_z \\ 0 & 0 & 0 \end{array} \right], \tag{2.3}$$

with

$$\begin{aligned} \theta_x &= u\tau_{xx} + v\tau_{xy} + w\tau_{xz} + \kappa \frac{\partial T}{\partial x}, \\ \theta_y &= u\tau_{yx} + v\tau_{yy} + w\tau_{yz} + \kappa \frac{\partial T}{\partial y}, \\ \theta_z &= u\tau_{zx} + v\tau_{zy} + w\tau_{zz} + \kappa \frac{\partial T}{\partial z}. \end{aligned} \tag{2.4}$$

Here, ρ_m, p, E_t, H, T and (u, v, w) are the mixture density, pressure, total energy, total enthalpy, temperature and velocity vector, respectively. Y_1 stands for the mass fraction of the gas phase. τ is the viscous tensor which can be formulated as follows if we assume Newtonian fluid and the Stokes hypotheses is valid.

$$\tau_{ij} = \mu \left(\frac{\partial u_i}{\partial x_j} + \frac{\partial u_j}{\partial x_i} - \frac{2}{3} \delta_{i,j} \frac{\partial u_k}{\partial x_k} \right). \tag{2.5}$$

The molecular viscosity coefficient μ and the thermal conductivity coefficient κ are computed based on the local mass fraction. $\mathbf{S}_{phasechange}$ represents the

source term vector corresponding to the transition rate from one phase to the other.

2.1.2 Determination of Mixture Properties

In homogeneous mixture equations, the mixture density, ρ_m, plays the role of mixture EOS:

$$\begin{aligned} \rho_m &= \tilde{\rho_l}\left(p,T\right)\left(1-\alpha_v\right)+\tilde{\rho_v}\left(p,T\right)\alpha_v, \\ \frac{1}{\rho_m} &= \frac{\left(1-Y_1\right)}{\tilde{\rho_l}\left(p,T\right)}+\frac{Y_1}{\tilde{\rho_v}\left(p,T\right)}. \end{aligned} \tag{2.6}$$

The subscript l and g stand for a property of liquid phase and gas phase, respectively. The density with tilde, $\tilde{\rho_l}$ and $\tilde{\rho_v}$, indicates the density of each phase on the occupied volume within a computational cell.

The mixture total enthalpy H and the mixture total energy E_t are calculated using the following relations. h is the specific enthalpy.

$$\begin{aligned} H &= h+\frac{1}{2}\left(u^2+v^2+w^2\right) \\ E_t &= H-\frac{p}{\rho_m} \\ h\left(p,T,Y_1\right) &= h_l\left(p,T\right)\left(1-Y_1\right)+h_v\left(p,T\right)Y_1 \end{aligned} \tag{2.7}$$

The mixture scalar quantities not specified are found based on the mass fraction for intensive properties and the volume fraction otherwise. Quantities of interest are specific heat, molecular and eddy viscosity, laminar and turbulent Prandtl number and thermal conductivity.

2.2 Preconditioning Techniques

Computational algorithms for compressible flows suffer from drastic deterioration of convergence rate and accuracy in calculating low speed flows. The

difference between the particle and acoustic speeds becomes huge at low Mach number limit. While the pseudo-time scales are decided based on the fastest characteristic speed, errors are convected at much lower particle speed, which causes detrimental effect on convergence rate [6]. This large disparity in system eigenvalues($u,\ u \pm c$) can be settled for steady low speed flows by premultiplying preconditioning matrix to the time derivative term.

The preconditioning matrix starts from the transformation matrix of the dependent variables in Eq. (2.1). From now on, we shall use primitive variable vector $\mathbf{W} = [p\ \ u\ \ v\ \ w\ \ T\ \ Y_1]^T$ instead of the conservative variables $\mathbf{Q}$ in Eq. (2.2) as the dependent variables. It is desirable to use p rather than ρ for computing incompressible flows. The transformation Jacobian $\mathbf{\Gamma_e} \equiv \partial\mathbf{Q}/\partial\mathbf{W}$ is given by

$$\mathbf{\Gamma_e} = \begin{bmatrix} \frac{\partial\rho_m}{\partial p} & 0 & 0 & 0 & \frac{\partial\rho_m}{\partial T} & \frac{\partial\rho_m}{\partial Y_1} \\ u\frac{\partial\rho_m}{\partial p} & \rho_m & 0 & 0 & u\frac{\partial\rho_m}{\partial T} & u\frac{\partial\rho_m}{\partial Y_1} \\ v\frac{\partial\rho_m}{\partial p} & 0 & \rho_m & 0 & v\frac{\partial\rho_m}{\partial T} & v\frac{\partial\rho_m}{\partial Y_1} \\ w\frac{\partial\rho_m}{\partial p} & 0 & 0 & \rho_m & w\frac{\partial\rho_m}{\partial T} & w\frac{\partial\rho_m}{\partial Y_1} \\ H\frac{\partial\rho_m}{\partial p} + \rho_m\frac{\partial H}{\partial p} - 1 & \rho_m u & \rho_m v & \rho_m w & H\frac{\partial\rho_m}{\partial T} + \rho_m\frac{\partial H}{\partial T} & H\frac{\partial\rho_m}{\partial Y_1} + \rho_m\frac{\partial H}{\partial Y_1} \\ Y_1\frac{\partial\rho_m}{\partial p} & 0 & 0 & 0 & Y_1\frac{\partial\rho_m}{\partial T} & \rho_m + Y_1\frac{\partial\rho_m}{\partial Y_1} \end{bmatrix}. \tag{2.8}$$

A slight touch on the Jacobian can make our system well-conditioned. We define the preconditioner as [8],

$$\mathbf{\Gamma} = \begin{bmatrix} \frac{1}{\beta} & 0 & 0 & 0 & \frac{\partial\rho_m}{\partial T} & \frac{\partial\rho_m}{\partial Y_1} \\ \frac{u}{\beta} & \rho_m & 0 & 0 & u\frac{\partial\rho_m}{\partial T} & u\frac{\partial\rho_m}{\partial Y_1} \\ \frac{v}{\beta} & 0 & \rho_m & 0 & v\frac{\partial\rho_m}{\partial T} & v\frac{\partial\rho_m}{\partial Y_1} \\ \frac{v}{\beta} & 0 & 0 & \rho_m & w\frac{\partial\rho_m}{\partial T} & w\frac{\partial\rho_m}{\partial Y_1} \\ \frac{H}{\beta} + \rho_m\frac{\partial H}{\partial p} - 1 & \rho_m u & \rho_m v & \rho_m w & H\frac{\partial\rho_m}{\partial T} + \rho_m\frac{\partial H}{\partial T} & H\frac{\partial\rho_m}{\partial Y_1} + \rho_m\frac{\partial H}{\partial Y_1} \\ \frac{Y_1}{\beta} & 0 & 0 & 0 & Y_1\frac{\partial\rho_m}{\partial T} & \rho_m + Y_1\frac{\partial\rho_m}{\partial Y_1} \end{bmatrix}. \tag{2.9}$$

It is observed that $\frac{\partial \rho_m}{\partial p}$ in $\mathbf{\Gamma_e}$ is replaced by a new term $\frac{1}{\beta}$ in $\mathbf{\Gamma}$, whereas every other term remains the same. The parameter $\frac{1}{\beta}$ can be regarded as pseudo-compressibility factor. If $\frac{1}{\beta} = \frac{\partial \rho_m}{\partial p}$, it is obvious that the system returns to the unpreconditioned original form.

The governing equations with this preconditioner turns

$$\mathbf{\Gamma}\frac{\partial \mathbf{W}}{\partial t} + \frac{\partial \left(\mathbf{F}^{(1)} - \mathbf{G}^{(1)}\right)}{\partial x} + \frac{\partial \left(\mathbf{F}^{(2)} - \mathbf{G}^{(2)}\right)}{\partial y} + \frac{\partial \left(\mathbf{F}^{(3)} - \mathbf{G}^{(3)}\right)}{\partial z} = \mathbf{S}_{phasechage}, \tag{2.10}$$

with the following resultant eigenvalues,

$$\lambda\left(\mathbf{\Gamma}^{-1}\frac{\partial \mathbf{F}^{(i)}}{\partial \mathbf{W}}\right) = U, U, U, U, U' + D, U' - D, \tag{2.11}$$

where,

$$U' = \frac{1}{2}\left(1 + \frac{c'^2}{c^2}\right)U,\ D = \frac{1}{2}\sqrt{\left(1 - \frac{c'^2}{c^2}\right)^2 U^2 + 4c'^2}, \tag{2.12}$$

$$c'^2 = \frac{\rho_m \frac{\partial h}{\partial T}}{\rho_m \frac{1}{\beta}\frac{\partial h}{\partial T} + \frac{\partial \rho_m}{\partial T}\left(1 - \rho_m \frac{\partial h}{\partial p}\right)}. \tag{2.13}$$

$\mathbf{F}^{(i)}$ and $\mathbf{G}^{(i)}$ $(i = 1, 2, 3)$ indicate the i-th column of the tensor $\mathbf{F}$ and $\mathbf{G}$. $U(= un_x + vn_y + wn_z)$ is the velocity component normal to a interface.

Our goal of preconditioning is to cluster eigenvalues to avoid the defects found in calculations of low speed flows. From Eq. (2.11) and (2.12), the only parameter in the preconditioned eigenvalues that can be arbitrarily defined regardless of the flow and thermodynamic conditions is c'. It can be easily deduced that the appropriate choice of c', hence appropriate choice of β, would help reach our goal. Eq. (2.13) is rearranged in terms of β in Ep. (2.14).

$$\frac{1}{\beta} = \frac{1}{c'^2} - \frac{\frac{\partial \rho_m}{\partial T}\left(1 - \rho_m \frac{\partial h}{\partial p}\right)}{\rho_m \frac{\partial h}{\partial T}} \tag{2.14}$$

Note that c' has a similar form with the original speed of sound c for general EOS in Eq. (2.15), except $\frac{\partial \rho_m}{\partial p}$ in c is replaced by $\frac{1}{\beta}$ in c'.

$$c^2 = \frac{\rho_m \frac{\partial h}{\partial T}}{\rho_m \frac{\partial \rho_m}{\partial p} \frac{\partial h}{\partial T} + \frac{\partial \rho_m}{\partial T} \left(1 - \rho_m \frac{\partial h}{\partial p}\right)}. \tag{2.15}$$

Therefore, we call c' pseudo-speed of sound or preconditioned speed of sound. Among a number of candidates for the preconditioned sound speed the following definition of c' is used.

$$c' = \min\left(c, \max\left(V, V_{ref}\right)\right). \tag{2.16}$$

$$V = \sqrt{u^2 + v^2 + w^2}. \tag{2.17}$$

If the local flow speed does not exceed the sonic speed, the preconditioned sound speed has the value of flow speed, not the physical sound speed. In supersonic region where $V \geq c$, the preconditioned sound speed becomes the physical sound speed. Through this type of cutting, all the system eigenvalues have the same order of magnitude in low Mach number regime. It should be pointed out that the preconditioned system is not right for unsteady low Mach number calculations since the preconditioning has altered the time accuracy of the original system by changing its eigenvalues.

Chapter 3

Numerical Methods

3.1 Extension of Two-phase RoeM and AUSMPW+ to General EOS

Before talking about the generalization of EOS-dependent term in two-phase RoeM and AUSMPW+ flux schemes, we will look at two-phase RoeM and AUSMPW+ first. Then, we will be able to pick out a term which is dependent on EOS, so that we could modify the term to improve two schemes to be employed with any kind of EOS. Both flux schemes have extended for two-phase flows from RoeM and AUSMPW+ schemes for compressible gas flows [2]. The original RoeM[9] and AUSMPW+[10] for gas dynamics are known to be efficient and accurate shock-stable schemes, and their two-phase versions also show efficient and accurate results for compressible two-phase flows.

3.1.1 Original Two-phase All-speed RoeM

Although Roe's FDS is widely used due to its accuracy, it suffers from carbuncle phenomena and being unable to filter out expansion shock from physical solutions. Analyzing the cause of carbuncle, RoeM suggests a Mach number based function f which controls the feeding rate of pressure perturbation to density field,

$$f = \begin{cases} 1 & \hat{u}^2 + \hat{v}^2 + \hat{w}^2 = 0 \\ |\hat{M}|^{h^*} & \text{elsewhere} \end{cases}, \tag{3.1}$$

$$h^* = 1 - \min\Big(\Pi^*_{i+1/2,j,k}, \Pi^*_{i,j+1/2,k}, \Pi^*_{i,j-1/2,k}, \Pi^*_{i+1,j+1/2,k}, \Pi^*_{i+1,j-1/2,k}, \Pi^*_{i,j,k+1/2}, \Pi^*_{i,j,k-1/2}, \Pi^*_{i+1,j,k+1/2}, \Pi^*_{i+1,j,k-1/2}\Big) \tag{3.2}$$

where $\hat{M} = \hat{U}/\hat{c}$. The variables with symbol hat for example, $\hat{U}, \hat{c}$, etc. are Roe-averaged values. Besides function f, RoeM adopts another Mach number based function g for the case in which pressure field is strongly and constantly perturbed like unsteady, high speed flows. The function g controls the damping rate of density field and restrains the pressure perturbation from consistent increase.

$$g = \begin{cases} 1 & \hat{M} = 0 \\ |\hat{M}|^{1-\Pi^*_{i+1/2,j,k}} & \hat{M} \neq 0 \end{cases}. \tag{3.3}$$

In the above two control functions f and g, a sensor of shock is needed to notice shock and practice appropriate amount of numerical dissipations. Such shock discontinuity sensing term(SDST) $\Pi^*_{1/2}$ is defined as below.

$$\Pi^*_{1/2} = \min\left(\frac{\bar{p}_L}{\bar{p}_R}, \frac{\bar{p}_R}{\bar{p}_L}\right), \ \bar{p}_{L,R} = \frac{1}{\frac{\alpha_{1,1/2}}{p_{L,R}} + \frac{1-\alpha_{1,1/2}}{p_{L,R}+p_c}}, \tag{3.4}$$

where $\alpha_{1,1/2}$ is the volume fraction of the gas phase at a cell interface. Note that in the original RoeM for gas dynamics, SDST is just a function of static pressure ratios. We will talk about SDST later in section 3.1.3.

With the modification for the preservation of total enthalpy in inviscid steady flow, the RoeM flux is written as the following form.

$$F_{1/2}^{(i)} = \frac{1}{b_1^* - b_2^*}\left[b_1^* F_L^{(i)} - b_2^* F_R^{(i)} + b_1^* b_2^* \left(\Delta Q^* - \frac{g}{1+|\tilde{M}^*|} B\Delta Q^{**}\right)\right], \quad (3.5)$$

$$\Delta Q^* = \begin{bmatrix} \Delta(\rho_m) \\ \Delta(\rho_m u) \\ \Delta(\rho_m v) \\ \Delta(\rho_m w) \\ \Delta(\rho_m H) \\ \Delta(\rho_m Y_1) \end{bmatrix}, \; B\Delta Q^{**} = \left(\Delta\rho_m - f\frac{\Delta p}{\hat{D}^2}\right) \begin{bmatrix} 1 \\ \hat{u} \\ \hat{v} \\ \hat{w} \\ \hat{H} \\ \hat{Y_1} \end{bmatrix} + \hat{\rho_m} \begin{bmatrix} 0 \\ \Delta u - n_x \Delta U \\ \Delta v - n_y \Delta U \\ \Delta w - n_z \Delta U \\ \Delta H \\ \Delta Y_1 \end{bmatrix}, \quad (3.6)$$

where $\tilde{M}^* = \text{sign}\left(\hat{M}^*\right) \times \min\left(1, |\hat{M}^*|\right), \hat{M}^* = \hat{U}'/\hat{D}$. Recall Eq. (2.11) for U' and D. For all-speed flow computations, all-speed extension strategy of HLLC (Harten-Lax-van Leer with Contact restoration scheme)-type by Luo *et al.* [11] has been implemented. The signal velocities for avoiding expansion shock of Roe's FDS and for positivity preserving property, are as below.

$$b_1^* = \max\left(\hat{U}' + \hat{D}, U_R' + \hat{D}, 0\right), b_2^* = \min\left(\hat{U}' - \hat{D}, U_L' - \hat{D}, 0\right) \quad (3.7)$$

3.1.2 Original Two-phase All-speed AUSMPW+

While AUSM+ improves the accuracy and shock instability of the AUSM scheme, it suffers from unwanted oscillation near the wall and overshoots behind a strong shock [12]. In order to prevent these, AUSMPW+ uses pressure based weighting function f which include pressure difference term to control numerical dissipations. Since excessive pressure difference term can cause a numerical instability, f needs to be limited near strong shock and stagnation point. In two-phase flows, near phase interface region should be also considered for the operation of f. The density is multiplied by the pressure difference term, and

the rapid change of density in distinct phases can make the numerical dissipation due to this pressure difference immoderate. Thus, the pressure based weighting function f^* in two-phase AUSMPW+ is achieved as follows:

$$f^*_{L,R} = \left(\frac{\bar{p}_{L,R}}{\bar{p}_s} - 1 \right) (1 - \omega_2) \frac{\min\left(\rho_{m,L}, \rho_{m,R}\right)}{\rho_{m,L,R}} \frac{1}{M_r^2}, \tag{3.8}$$

where, $M_r^2 = c'^2/c^2$. Unlike AUSM+ method which uses one-sided property only, AUSMPW+ scheme utilizes another pressure based weighting function ω to get rid of overshoots behind shock by considering both-side properties.

$$\omega = \max\left(\omega_1, \omega_2\right), \ \omega_1 = 1 - {\Pi^*_{1/2}}^3, \ \omega_2 = 1 - \left(\frac{\min\left(\bar{p}_{1,L}, \bar{p}_{1,R}, \bar{p}_{2,L}, \bar{p}_{2,R}\right)}{\max\left(\bar{p}_{1,L}, \bar{p}_{1,R}, \bar{p}_{2,L}, \bar{p}_{2,R}\right)} \right)^2. \tag{3.9}$$

$\bar{p}_{L,R}$ properties and SDST $\Pi^*_{1/2}$ in f^* and ω are same as in two-phase all-speed RoeM scheme, Eq. (3.4).

With the pressure based weighting functions, AUSMPW+ scheme is formulated as

$$F^{(i)}_{1/2} = \bar{M}^{*+}_L c^*_{1/2} Q_L + \bar{M}^{*-}_R c^*_{1/2} Q_R + \left(P^{*+}_L p_L + P^{*-}_R p_R \right). \tag{3.10}$$

For all-speed flow calculations, the scaling technique of Edwards and Liou [13] reflecting the preconditioned system eigenvalues has been adopted. Mach number and pressure splitting functions $\bar{M}^{*\pm}_{L,R}$ and $P^{*\pm}_{L,R}$ are obtained using the following scaled Mach number:

$$M^{**}_{L,R} = \frac{1 + M^2_{r,1/2}}{2} \times \frac{M_{L,R}}{\phi_{1/2}} + \frac{1 - M^2_{r,1/2}}{2} \times \frac{M_{R,L}}{\phi_{1/2}}. \tag{3.11}$$

The function $\phi_{1/2}$ is introduced to reflect the preconditioned eigenvalues.

$$\phi_{1/2} = \frac{M_{1/2}}{M^*_{1/2}} = \frac{\sqrt{\left(1 - M^2_{r,1/2}\right) M^2_{1/2} + 4 M^2_{r,1/2}}}{1 + M^2_{r,1/2}} \tag{3.12}$$

$$M_{L,R}^{*\pm} = \begin{cases} \pm\frac{1}{4}\left(M_{L,R}^{**} \pm 1\right)^2 & |M_{L,R}^{**}| \le 1 \\ \frac{1}{2}\left(M_{L,R}^{**} \pm |M_{L,R}^{**}|\right) & |M_{L,R}^{**}| > 1 \end{cases} \tag{3.13}$$

$$P_{L,R}^{*\pm} = \begin{cases} \pm\frac{1}{4}\left(M_{L,R}^{**} \pm 1\right)^2 \left(2 \mp M_{L,R}^{**}\right) \pm \alpha M_{L,R}^{**}\left(M_{L,R}^{**\,2} - 1\right)^2 & |M_{L,R}^{**}| \le 1 \\ \frac{1}{2}\left(1 \pm \mathrm{sign}\left(M_{L,R}^{**}\right)\right) & |M_{L,R}^{**}| > 1 \end{cases} \tag{3.14}$$

(i) for $M_{1/2} \ge 0$

$$\begin{aligned} \bar{M}_L^{*+} &= M_L^{*+} + M_R^{*-}\left[(1-\omega)\left(1+f_R^*\right) - f_L^*\right], \\ \bar{M}_R^{*-} &= M_R^{*-}\omega\left(1+f_R^*\right). \end{aligned} \tag{3.15}$$

(ii) for $M_{1/2} < 0$

$$\begin{aligned} \bar{M}_L^{*+} &= M_L^{*+}\omega\left(1+f_L^*\right), \\ \bar{M}_R^{*-} &= M_R^{*-} + M_L^{*+}\left[(1-\omega)\left(1+f_L^*\right) - f_R^*\right]. \end{aligned}$$

The choice of numerical speed of sound is crucial to capture discontinuity accurately in AUSM-type schemes. Unlike in gas dynamics, there is no Prandtl relation for general two-phase flows. Therefore, two-phase AUSMPW+ cannot use the interfacial speed of sound of original AUSMPW+ defined for gas dynamics satisfying Prandtl relation. To be consistent with the physical speed of sound at mixture flows, two-phase AUSMPW+ uses Roe-averaged enthalpy and mass fraction for the calculation of interfacial speed of sound $c_{1/2}$. The scaled interfacial speed of sound in Eq. (3.10) is defined using $\phi_{1/2}$ to reflect preconditioned system eigenvalues.

$$c_{1/2}^* = c_{1/2} \times \phi_{1/2}. \tag{3.16}$$

3.1.3 Generalization of SDST

RoeM and AUSMPW+ methods both have SDST in their Mach number based or pressure based functions to provide appropriate numerical dissipations at

problematic regions. The original SDST in RoeM and AUSMPW+ for gas dynamics senses these problematic regions through static pressure ratios across a cell interface in the following manner:

$$\Pi_{1/2} = \min\left(\frac{p_L}{p_R}, \frac{p_R}{p_L}\right). \tag{3.17}$$

As can be seen in Eq. (3.17), SDST is designed to be near zero when shock is present, and near one in the smooth region. Inaccurate value of SDST causes improper amount of numerical dissipations, which incurs numerical instability or overly dissipative solutions.

The problem appears if we try to apply this SDST to two-phase computations as it is. Due to the large disparity of density between different phases, the dynamic pressure changes rapidly across a phase interface and so does the static pressure. Because the pressure field changes drastically near phase interface even for non-shock region, original SDST has trouble in distinguishing shock discontinuity and phase interface. Two-phase SDST in Eq. (3.4) is defined to handle this trouble with the assumption of specific EOSs [2].

$$\Pi^*_{1/2} = \min\left(\frac{\bar{p}_L}{\bar{p}_R}, \frac{\bar{p}_R}{\bar{p}_L}\right), \ \bar{p}_{L,R} = \frac{1}{\frac{\alpha_{1,1/2}}{p_{L,R}} + \frac{1-\alpha_{1,1/2}}{p_{L,R}+p_c}}$$

The term of our interest is p_c. This term originates from the stiffened EOS for liquid water. Several other EOSs, namely Tait's EOS, the van der Waals EOS and the Peng-Robinson EOS can be also used as they have a term similar to p_c. However, this is not enough for general all-speed two-phase computations.

As mentioned in Chapter 1, these several EOSs cannot cover all types of fluids we are interested in. That is, our two-phase RoeM and AUSMPW+ methods cannot perform properly with other working fluids such as cryogens or liquid fuels. To remove this restriction, we design a new two-phase SDST which does

not contain a term dependent on specific EOSs as below.

$$\Pi^{**}_{1/2} = \min\left(\frac{\bar{p}^*_L}{\bar{p}^*_R}, \frac{\bar{p}^*_R}{\bar{p}^*_L}\right), \ \bar{p}^*_{L,R} = p_{L,R} + \rho_{m,1/2} c^2_{1/2}. \tag{3.18}$$

Here, newly defined leveled pressure $\bar{p}^*_{L,R}$ is free from EOS-dependent term p_c. It only requires the mixture density and speed of sound at a cell interface which are irrespective of the form of EOS.

The capability of the new two-phase SDST for RoeM and AUSMPW+ must be examined if it captures a shock discontinuity only, without confusing with the phase interface in two-phase flows. The behavior of SDSTs, $\Pi_{1/2}$, $\Pi^*_{1/2}$, $\Pi^{**}_{1/2}$, are observed for water-gas one-dimensional mixture shock conditions. Table 3.1 shows the inverse values of the SDSTs in terms of the mass fraction of the gas phase with $M_L = 1.5,\ 2.0$ and 6.0. In the first column, "liquid" means pure liquid phase of $Y_1 = 0.0$ and "gas" means pure gas phase of $Y_1 = 1.0$. The original SDST for gas dynamics $\Pi_{1/2}$ shows poor performance with exceedingly large inverse values as the mass fraction Y_1 decreases near pure water. For higher Mach number case, this situation becomes worse for $\Pi_{1/2}$. On the contrary, two-phase SDSTs $\Pi^*_{1/2}$, $\Pi^{**}_{1/2}$ provide almost uniform values throughout the whole range of mass fraction for all cases of Mach number. Figure 3.1 confirms this tendency again. From this results, it can be concluded that $\Pi^{**}_{1/2}$ can be used consistently for all mixture fluid flows regardless of the mixture density and speed of sound with any type of fluids.

We will use this new two-phase SDST $\Pi^{**}_{1/2}$ in control functions of two-phase RoeM and AUSMPW+ schemes for solving all test cases in this study hereafter.

Table 3.1: Inverse values of the SDSTs for the 1-D shock relation

(subscript "L" indicates pre-shock value)

$\log(Y_1)$	$\rho_{m,L}$ (kg/m^3)	c_L (m/s)	$M_L = 1.5$			$M_L = 2.0$			$M_L = 6.0$		
			$1/\Pi_{1/2}$	$1/\Pi^{*}_{1/2}$	$1/\Pi^{**}_{1/2}$	$1/\Pi_{1/2}$	$1/\Pi^{*}_{1/2}$	$1/\Pi^{**}_{1/2}$	$1/\Pi_{1/2}$	$1/\Pi^{*}_{1/2}$	$1/\Pi^{**}_{1/2}$
liquid	1000.00	1458.95	6565.69	3.18750	1.62494	15756.3	6.25000	2.49986	183812	62.2500	18.4983
-8	999.99	1347.99	4836.94	2.61162	1.53927	12682.5	5.22595	2.41416	156147	53.0312	18.4124
-7	999.92	885.63	8.24318	1.22860	1.00187	2494.80	1.83307	1.64421	64413.2	22.4672	17.6392
-6	999.19	342.81	2.42609	2.06508	1.00246	4.84434	2.78550	1.00662	5213.17	2.75372	9.97992
-5	991.91	112.01	2.26608	2.22898	1.02029	4.06936	3.83132	1.04918	44.8567	5.75330	1.70267
-4	924.61	38.10	2.25124	2.24752	1.16414	4.00529	3.98094	1.39424	36.5598	23.9056	5.66480
-3	550.87	20.23	2.24981	2.24943	1.59168	3.99909	3.99665	2.41982	35.8958	34.1280	17.5202
-2	109.25	32.26	2.25005	2.25001	1.80068	3.99940	3.99915	2.92118	35.8416	35.6551	23.3168
-1	12.12	92.31	2.25426	2.25426	1.83092	4.00948	4.00946	2.99373	35.9547	35.9338	24.1568
gas	1.225	340.29	2.45833	2.45833	1.85784	4.50000	4.50000	3.05882	41.8333	41.8333	25.0196

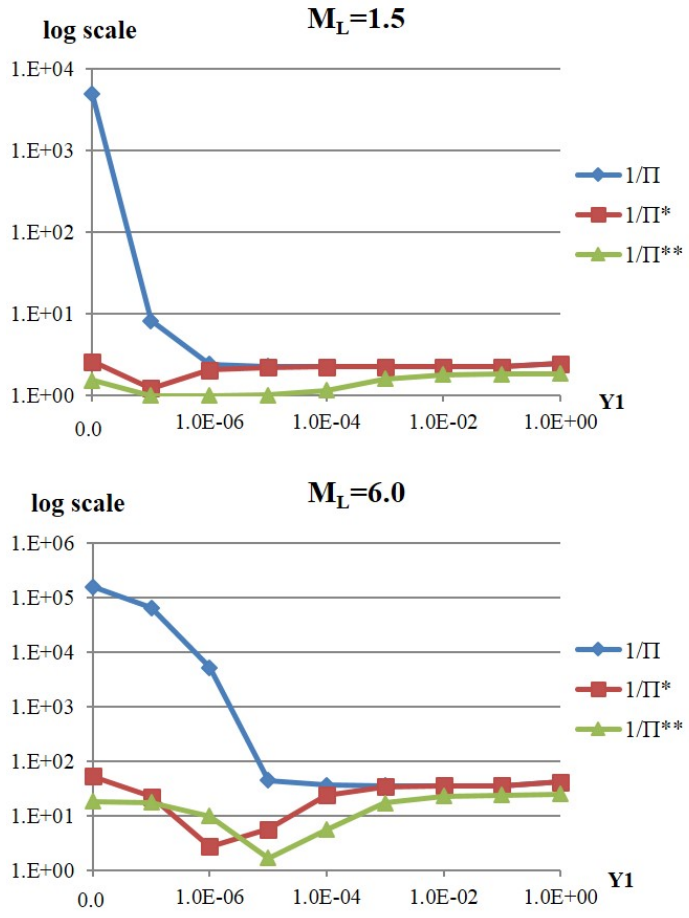

Figure 3.1: Inverse values of the SDSTs for the 1-D shock relation

3.2 System Preconditioning for Unsteady Flows

As seen in section 2.2, conventional preconditioning technique applies to steady computations. Since the preconditioner manipulates system eigenvalues to enhance convergence rate in low Mach number flows, applying preconditioner, by nature, destroys the time accuracy of the original system. Hence, the employment of the current preconditioning method as it is in unsteady flows is absurd. The preconditioning matrix is decided according to one preconditioning parameter, the preconditioned speed of sound or pseudo-speed of sound, c' in Eq. (2.16). If $c' = c$, then the pseudo-compressibility factor $\frac{1}{\beta}$ is restored to the original $\frac{\partial \rho_m}{\partial p}$, which leads the preconditioning matrix Γ to revert to the transformation Jacobian $\Gamma_e = \frac{\partial \mathbf{Q}}{\partial \mathbf{W}}$. In this sense, we can redefine c' as follows:

$$c'_{no} = c \qquad \text{no preconditioning,} \tag{3.19}$$

$$c'_{steady} = \min\left(c, \max\left(V, V_{ref}\right)\right) \quad \text{steady preconditioning.} \tag{3.20}$$

While preconditioning has proved to be highly successful for steady flows, extending preconditioning to unsteady flows is still struggling. In unsteady flows, waves propagate both in pseudo-time and physical time. As the relevant physical time scale becomes small, physical acoustic waves are of primary consideration unlike in steady flows. The difficulty of unsteady preconditioning comes from the fact that the present steady preconditioning is so dissipative at low Mach number limit for the pressure field that it cannot resolve the acoustic time scale properly which is dominant in unsteady flows characterized by high Strouhal number. Therefore, for low Mach high Strouhal number flows, the system should be restored to its original unpreconditioned form to properly capture the physical acoustic waves with good convergence. In order to achieve effective preconditioning, we need more general unsteady preconditioning parameter which takes Strouhal number into account. The unsteady preconditioned speed

of sound should turn off the preconditioning for high Strouhal number flows, and must revert to the conventional steady preconditioned speed of sound as the Strouhal number decreases.

We use local Strouhal number in the following form:

$$Str = \frac{L_{chr}}{\pi \Delta t V}, \tag{3.21}$$

where L_{chr} is a characteristic length scale usually set as the domain size, Δt is the physical time step size. Flows with small physical time scale refer to high Strouhal number flows. Δt is determined with the following CFL-like condition.

$$CFL_{\mathcal{U}} = \frac{\mathcal{U} \Delta t}{\Delta x}, \tag{3.22}$$

where $\mathcal{U}$ is velocity scale of our interest and Δx is typically taken as the average cell width. The velocity scale $\mathcal{U}$ can be chosen to be either the particle speed (CFL_V) or the acoustic speed (CFL_c). We choose CFL_c in the case of flows with small physical time scale, i.e., high Strouhal number flows. In other words, if the acoustic wave is dominant in flows, we focus on the resolution of acoustic time scale. The value of $CFL_{\mathcal{U}}$ is fixed as unity. The wave of our consideration, particle if CFL_V and acoustic wave if CFL_c, moves a distance of 1 cell per time step under the condition of $CFL = 1$.

In this light, we can define an unsteady preconditioned speed of sound.

$$c'_{unsteady} = \min\left(c, \max\left(V, Str \times V, V_{ref}\right)\right) \tag{3.23}$$

It can be observed that when Strouhal number is high enough, $c'_{unsteady}$ becomes $c'_{no}(= c)$, the original speed of sound, and it restores the system to the original unpreconditioned formation. As Strouhal number becomes small, $c'_{unsteady}$ becomes c'_{steady}, and the clustering of system eigenvalues is attained. This behavior of preconditioned speed of sound is illustrated in Figure 3.2,

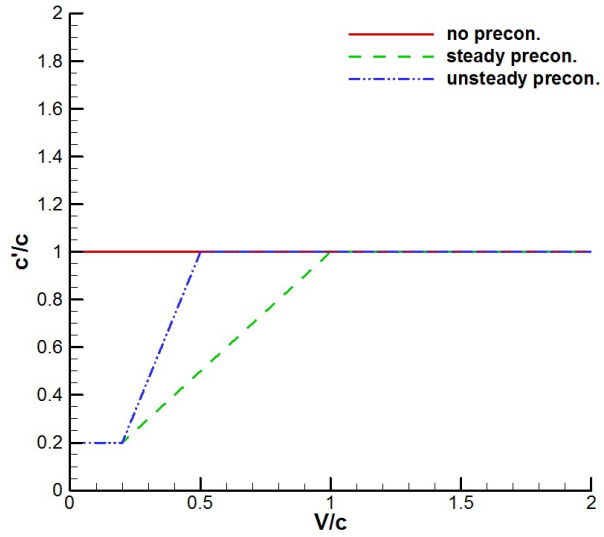

Figure 3.2: Preconditioned sound speed according to local velocity

where V_{ref}/c is set to 0.2. If there is no preconditioning applied, c' remains the same as the physical speed of sound c, regardless of the flow speed. In the case of steady preconditioning, the preconditioned speed of sound has the value of local flow speed in subsonic region, and returns to the physical speed of sound in supersonic region. The unsteady preconditioning brings this return forward. Although the local flow speed is less than sonic speed, the preconditioned speed of sound reverts to the physical speed of sound to restore the system into its original time-accurate form. In this way, the effective unsteady preconditioning is accomplished with the unsteady preconditioning parameter Eq. (3.23).

3.3 Scaling of Numerical Dissipations

The system preconditioning parameter, whether it is steady or unsteady, affects not only the convergence of the system, but also the numerical dissipations in flux functions if the local velocity is below certain cutting values represented in

Figure 3.2. Since the flux functions are multiplied by the inverse of the preconditioning matrix, the scaling of numerical dissipations becomes dependent on the preconditioned speed of sound, naturally.

Low Mach limit	Low Strouhal limit		High Strouhal limit	
Formulation	Pressure	Velocity	Pressure	Velocity
No preconditioning	O(M)	O(1/M)	O(1)	O(1/M)
Steady preconditioning	O(1)	O(1)	O(1/M)	O(1)
Unsteady preconditioning	O(1)	O(1)	O(1)	O(1/M)

Table 3.2: Preconditioning effects on artificial dissipation scaling of FDS [5]

Table 3.2 shows the preconditioning effects on artificial dissipation scaling of flux difference algorithms. As appeared in the table, low Mach high Strouhal number flows resolve the physical acoustic time scale properly with appropriate amount of numerical dissipation in pressure field through unsteady preconditioning. However, the numerical dissipation of velocity field becomes too much as the Mach number becomes small. If we use steady preconditioned speed of sound for low Mach high Strouhal number flows, the situation is reversed. The numerical dissipation in velocity field is well scaled while the pressure field suffers from excessive dissipation. Without preconditioning generates the same problem as in unsteady preconditioning, since the unsteady preconditioning forces the system to be unpreconditioned. That is, even if we do not concern about the convergence rate, the accuracy of the solution is always damaged for unsteady low Mach number flows with or without preconditioning.

In addition to the accuracy problem, numerical instability issue is also raised in low Mach number flows. In slowly moving flows, the checkerboard instability is witnessed for some all-speed schemes due to the deficient coupling of pres-

sure and velocity field. According to the recent study, the preconditioned Roe has proved to be the best for avoiding checkerboard among various Roe-type schemes [7]. To completely suppress the checkerboard, a numerical flux scheme needs to have same form of numerical dissipations as that of the preconditioned Roe. To sum up, numerical dissipations in previous RoeM and AUSMPW+ methods should be modulated in some way to avoid accuracy and stability problem mentioned above in low Mach number limit while leaving the system preconditioning part untouched for the convergence of steady/unsteady low Mach number flows.

Breakthroughs for the accuracy degradation problem of low Mach high Strouhal number flows have been suggested by researchers. For flux difference schemes, the blended scheme which takes the unsteady preconditioning for pressure and steady preconditioning for velocity has been proposed [4], [5]. For flux splitting schemes, an idea which is to tailor dissipations for pressure and velocity unsteadiness independently has been applied to AUSM+-up [4], [5] and CUSP[6]. Since the scaled AUSM+-up or CUSP outperforms the blended scheme, we shall apply the scaling idea to two-phase AUSMPW+ to get rid of accuracy degradation in low Mach number limit.

Apart from system preconditioning, a separate research has focused on the scaling of numerical dissipations of Roe-type all-speed schemes [7]. This study has scrutinized each term in numerical dissipations of several flux difference schemes, and found out which term causes numerical instability and accuracy degradation in low Mach number region. With the proper scaling of the targets, they have succeeded to exclude the troubles of accuracy and stability. The idea of this study will be applied to two-phase RoeM.

Examining two strategies for AUSM-type and Roe-type found in separate researches, it is discovered that their approaches are eventually the same. The

key is the inclusion and exclusion of global cut-off value in scaling parameter. In preconditioning technique, global cut-off value is introduced to prevent numerical instability which occurs when dissipation is scaled near zero at stagnation region. In section 3.2, V_{ref} is such global cut-off in Eq. (3.20) and Eq. (3.23). Without extra treatment on numerical dissipations, the conventional preconditioning technique has employed the preconditioned speed of sound with global-cutoff in evaluating system eigenvalues and numerical dissipations uniformly. But, according to the strategy from the analysis of Roe-type schemes, global cut-off is unnecessary in the numerator of the numerical dissipations.

Resultant numerical dissipation with this strategy can be formulated as follows for Roe-type scheme.

$$F_d = -\frac{1}{2}\left\{ |U| \begin{bmatrix} \Delta\rho \\ \Delta(\rho u) \\ \Delta(\rho v) \\ \Delta(\rho w) \\ \Delta(\rho E_t) \end{bmatrix} + \delta U \begin{bmatrix} \rho \\ \rho u \\ \rho v \\ \rho w \\ \rho H \end{bmatrix} + \delta p \begin{bmatrix} 0 \\ n_x \\ n_y \\ n_z \\ U \end{bmatrix} \right\}, \tag{3.24}$$

$$\delta U = \left(D' - \frac{1-\theta'}{2} U \frac{U'}{D'} - \theta' |U| \right) \frac{\Delta p}{\rho c'^2} + \frac{\tilde{U}}{D'} \Delta U, \tag{3.25}$$

$$\delta p = \frac{\tilde{U}}{D'} \Delta p + \left(\tilde{D} - |U| + \frac{1-\tilde{\theta}}{2} U \frac{\tilde{U}}{D'} \right) \rho \Delta U. \tag{3.26}$$

Here, the prime symbol " $\prime$ " indicates a variable from the preconditioned speed of sound with global cut-off, while the tilde symbol "$\sim$" indicates a variable from the preconditioned speed of sound without global cut-off.

$$\begin{array}{ll} c' = \min\left(c, \max\left(V, Str \times V, V_{ref}\right)\right) & \tilde{c} = \min\left(c, V\right) \\ \theta' = \frac{c'^2}{c^2} & \tilde{\theta} = \frac{\tilde{c}^2}{c^2} \\ U' = \frac{1}{2}\left(1+\theta'\right) U & \tilde{U} = \frac{1}{2}\left(1+\tilde{\theta}\right) U \\ D' = \frac{1}{2}\sqrt{4c'^2 + \left(1-\theta'\right)^2 U^2} & \tilde{D} = \frac{1}{2}\sqrt{4\tilde{c}^2 + \left(1-\tilde{\theta}\right)^2 U^2} \end{array} \tag{3.27}$$

In numerical dissipations Eq. (3.25) and Eq. (3.26), the prime variables are all in the denominator and tilde variables are in numerator except for the coefficient of pressure difference term in δU. This part is the only exception to be consistent with the numerical dissipation of preconditioned Roe for suppressing checkerboard instability, as mentioned earlier.

In AUSM-type ideas, a scaling factor with Strouhal number is dividing and scaling factor without Strouhal number is multiplying. That is to say, Strouhal number is functioning as global cut-off value in this case. Numerical dissipations of AUSM-type with corresponding strategy is written as,

$$D_p = \frac{K_p}{\phi'_{1/2}} \frac{\max(1 - \sigma \bar{M}_e^2, 0)}{\bar{\rho}\bar{c}^2} \Delta p, \tag{3.28}$$

$$D_u = -2K_u P^+ P^- \bar{\rho} \tilde{\phi}_{1/2} \bar{c} \Delta u. \tag{3.29}$$

M_e is local Mach number. Here, the scaling factor is ϕ. The rule of nomenclature for " $\prime$ " and "$\sim$" applies identically.

$$\begin{aligned} M_o'^2 &= \min(1, \max(\bar{M}_e^2, \bar{M}_e^2 Str^2)) \quad & \tilde{M}_o^2 &= \min(1, \bar{M}_e^2) \\ \phi'_{1/2} &= M'_o(2 - M'_o) & \tilde{\phi}_{1/2} &= \tilde{M}_o(2 - \tilde{M}_o) \end{aligned} \tag{3.30}$$

3.3.1 Properly Scaled Two-phase All-speed RoeM

Two-phase RoeM is newly derived recently since the numerical dissipation of the first version of two-phase RoeM [2] which used HLLC-type all-speed extension [11] is not the same form of the preconditioned Roe. Note that the preconditioned Roe is better than the preconditioned HLLC scheme for avoiding checkerboard instability [7]. Refer to Kim *et al.* [1] for detailed derivation process. In this study, the scaling strategy we have examined in section 3.3 is applied to the numerical dissipation of the newly derived two-phase RoeM.

Following is the properly scaled two-phase all-speed RoeM scheme.

$$F_{1/2}^{(i)} = \frac{1}{b_1 - b_2}\left[b_1 F_L^{(i)} - b_2 F_R^{(i)} + \widetilde{b_1 b_2}\Delta Q^* - \widetilde{b_1 b_2}\frac{g}{\tilde{c}^* - \tilde{M}^*\tilde{U}} B\Delta Q'^{**}\right], \quad (3.31)$$

$$B\Delta Q'^{**} = \left(C_{\rho_m}\Delta\rho_m - fC_p\frac{\Delta p}{\hat{c}'^2}\right)\begin{bmatrix}1\\ \hat{u}\\ \hat{v}\\ \hat{w}\\ \hat{H}\\ \hat{Y}_1\end{bmatrix} + \hat{\rho}_m C_{\rho_m}\begin{bmatrix}0\\ \Delta u - n_x\Delta U\\ \Delta v - n_y\Delta U\\ \Delta w - n_z\Delta U\\ \Delta H\\ \Delta Y_1\end{bmatrix}, \quad (3.32)$$

where,

$$C_{\rho_m} = \tilde{c}^* - |\hat{U}| + \tilde{\alpha}\hat{U}\hat{\tilde{M}}^*,\ C_p = c'^* - \big(1 - 2\tilde{\alpha}\big)|\hat{U}| - \tilde{\alpha}\hat{U}\hat{\tilde{M}}^*. \quad (3.33)$$

For unified notation with previous section, prime and tilde variables are defined depending on the inclusion of global cut-off value, i.e., Str, V_{ref}.

$$c'^2 = \begin{cases} c^2 & \text{no precon.} \\ \min(c^2, \max(V^2, V_{ref}^2)) & \text{steady precon.} \\ \min(c^2, \max(V^2, Str \times V^2, V_{ref}^2)) & \text{unsteady precon.} \end{cases}$$
$$\tilde{c}^2 = \begin{cases} c^2 & \text{no precon.} \\ \min(c^2, V^2) & \text{steady/unsteady precon.} \end{cases} \quad (3.34)$$

$$\begin{aligned} U' &= \tfrac{1}{2}(1 + \tfrac{c'^2}{c^2})U, & \tilde{U} &= \tfrac{1}{2}(1 + \tfrac{\tilde{c}^2}{c^2})U \\ D' &= \tfrac{1}{2}\sqrt{\left(1 - \tfrac{c'^2}{c^2}\right)^2 U^2 + 4c'^2}, & \tilde{D} &= \tfrac{1}{2}\sqrt{\left(1 - \tfrac{\tilde{c}^2}{c^2}\right)^2 U^2 + 4\tilde{c}^2} \\ M'^* &= \tfrac{|U'+D'|-|U'-D'|}{2D'}, & \tilde{M}^* &= \tfrac{|\tilde{U}+D'|-|\tilde{U}-D'|}{2D'} \\ c'^* &= \tfrac{|\tilde{U}+D'|-|\tilde{U}-D'|}{2}, & \tilde{c}^* &= \tfrac{|\tilde{U}+\tilde{D}|-|\tilde{U}-\tilde{D}|}{2} \\ \alpha' &= \tfrac{1}{2}(1 - \tfrac{c'^2}{c^2}), & \tilde{\alpha} &= \tfrac{1}{2}(1 - \tfrac{\tilde{c}^2}{c^2}) \end{aligned} \quad (3.35)$$

The rule says that the global cut-off is unnecessary in numerator of the numerical dissipation, except the coefficient of the pressure difference term. Our

scaling is following the rule. The coefficient of the pressure difference term is $C_p/\hat{c}'^2$. The denominator is the preconditioned sound speed with global-cut off. Every other term in numerator is tilde value which comes from preconditioned sound speed without global cut-off. C_p has to be the exception of the rule to avoid instability, but through our experiment, exception of only c^* is enough for C_p in Eq. (3.33).

The signal velocities is also redefined to follow the rule. A little trick is made here. If we define $b_1 b_2$ by Eq. (3.37) not by just simple multiplication, D' is located in denominator and $\tilde{D}$ in numerator through $\widetilde{b_1 b_2}/(b_1 - b_2)$.

$$b_1 = \max(\hat{\tilde{U}} + \hat{D}', \tilde{U}_R + \hat{D}', 0),\ b_2 = \min(\hat{\tilde{U}} - \hat{D}', \tilde{U}_L - \hat{D}', 0) \tag{3.36}$$

$$\widetilde{b_1 b_2} = b_1 b_2 + D'^2 - D'\tilde{D} \tag{3.37}$$

Finally, the Mach number based functions are calculated with the new two-phase SDST $\Pi^{**}_{1/2}$ to extend the numerical method to general EOS.

$$f = f(\Pi^{**}_{1/2}),\ g = g(\Pi^{**}_{1/2}) \tag{3.38}$$

3.3.2 Properly Scaled Two-phase All-speed AUSMPW+

The previous extension of AUSMPW+ to two-phase flows [2] borrows the scaling technique of Edwards and Liou [13]. However, the calculations of Mach number and pressure splitting functions are inefficient due to the use of complex scaled Mach number instead of the original one. For the efficient calculation, Kim *et al.* [1] deserted the scaled Mach number, and introduces extra velocity difference term to the pressure dissipation, as proposed in AUSM+-up scheme [14]. The rule for the scaling of numerical dissipations discussed in section 3.3 is applied to the newly defined two-phase AUSMPW+.

$$F^{(1)}_{1/2} = \bar{M}^+_L c_{1/2} Q_L + \bar{M}^-_R c_{1/2} Q_R + P^+_L p_L + P^-_R p_R + D_u, \tag{3.39}$$

where,

$$D_u = -K_u P_L^+ P_R^- (\rho_{m,R} + \rho_{m,L}) \tilde{\phi}_{1/2} c_{m,1/2} (u_R - u_L). \tag{3.40}$$

The Mach number and pressure splitting functions $\bar{M}_{L,R}^{\pm}$ and $P_{L,R}^{\pm}$ are obtained using original Mach number. The pressure based weighting function f and ω are calculated with the new two-phase SDST $\Pi_{1/2}^{**}$.

$$f'_{L,R} = (\frac{\bar{p}^*_{L,R}}{\bar{p}^*_s} - 1)(1 - \omega_2) \frac{1}{\phi'_{1/2}} \tag{3.41}$$

$$\omega = \max(\omega_1, \omega_2),\ \omega_1 = 1 - {\Pi_{1/2}^{**}}^3,\ \omega_2 = 1 - \left(\frac{\min\left(\bar{p}^*_{1,L}, \bar{p}^*_{1,R}, \bar{p}^*_{2,L}, \bar{p}^*_{2,R}\right)}{\max\left(\bar{p}^*_{1,L}, \bar{p}^*_{1,R}, \bar{p}^*_{2,L}, \bar{p}^*_{2,R}\right)} \right)^2. \tag{3.42}$$

The scaling parameter ϕ is defined as follows.

$$\phi'_{1/2} = M'_o(2 - M'_o), \quad \tilde{\phi}_{1/2} = \tilde{M}_o(2 - \tilde{M}_o) \tag{3.43}$$

$$M'^2_o = \begin{cases} 1 & \text{no precon.} \\ \min(1, \max(\frac{V^2}{c^2}, \frac{V^2_{ref}}{c^2})) & \text{steady precon.} \\ \min(1, \max(\frac{V^2}{c^2}, Str^2 \times \frac{V^2}{c^2}, \frac{V^2_{ref}}{c^2})) & \text{unsteady precon.} \end{cases}$$

$$\tilde{M}^2_o = \begin{cases} 1 & \text{no precon.} \\ \min(1, \bar{M}^2) & \text{steady/unsteady precon.} \end{cases} \tag{3.44}$$

$$\bar{M}^2 = \frac{1}{2}(M_L^2 + M_R^2) \tag{3.45}$$

The numerical dissipations of two-phase RoeM and AUSMPW+ schemes are hereby scaled properly for all-speed flow calculations. Furthermore, the form of numerical dissipation of two-phase RoeM takes after that of the preconditioned Roe, so that our numerical method becomes free from checkerboard instability in low Mach number flows. Also, flux calculations of AUSMPW+ scheme becomes much easier and efficient.

Chapter 4

Numerical Results

The newly designed two-phase SDST $\Pi^{**}_{1/2}$ and the system preconditioning with the scaling of numerical dissipations discussed in chapter 3 are verified with various numerical tests in this chapter. The system preconditioning and the scaling of numerical dissipations are validated in single phase first. Then, two-phase problems are computed with new SDST as well as preconditioning.

- Spatial discretization
  - Numerical flux functions: properly scaled two-phase all-speed RoeM, AUSMPW+
  - Higher-order extension: 5th order interpolation with MLP (MLP5) [15], MUSCL approach [16] with TVD limiter
- Time integration
  - Unsteady computation: 3rd order TVD Runge-Kutta method
  - Implicit time integration for steady computation : LU-SGS [17]

4.1 Single-phase Flow Computation

4.1.1 Steady Inviscid Flow over a NACA0012 Airfoil

The two-dimensional transonic Euler flow past an airfoil is simulated with M_∞ 0.8 and angle of attack 1.25°, with the 513x153 O-type grid. MLP5 is used for more accurate computation. Since the flow condition is transonic, the system preconditioning is not needed. We can verify the scaling of numerical dissipation which is performed for low Mach number region, has nothing to do with moderate to high Mach number region. We compare the results with and without scaling of numerical dissipations.

Table 4.1 represents C_L and C_D results of present study. It can be seen that the results with scaling of numerical dissipation is similar to the results without scaling. These results are also comparable to the reference values. The reference values in the last column of Table 4.1 is the averages in the continuum level of Table 4.2. Figure 4.1 also shows almost identical pressure contours of with and without scaling of numerical dissipations of present study.

4.1.2 Steady Viscous Flow over a RAE2822 Airfoil

Along with the inviscid transonic flow, a viscous transonic flow over an airfoil is computed as well. The computation is performed with 368x64 C-type grid points at p=108987.39 Pa, T=255.56 K, M_∞=0.729, angle of attack=2.31°. $k-\omega$ SST turbulence model [19] is employed and MLP5 is used for high order accuracy. System preconditioning is not required.

The pressure coefficient curves are drawn in Figure 4.2. Although CFD results somewhat strayed from the experimental result near shock, they are very close to each other regardless of the scaling of numerical dissipations. Also the results of present study coincide with the reference CFD data (WIND).

Through this two transonic flow computations, we confirmed that the scaling of numerical dissipations does not affect inviscid or viscous flows with fairly over low Mach number.

	Without scaling		With scaling		Reference
	RoeM	AUSMPW+	RoeM	AUSMPW+	
C_L	0.3499	0.3467	0.3486	0.3526	0.3519
C_D	0.0224	0.0222	0.0223	0.0226	0.0226

Table 4.1: C_L, C_D of NACA0012 - present

NC NC^2		FLO82-HCUSP	OVERFLOW V2.1t	CFL3Dv6	CFL3Dv6+ Vortex
256	C_L	0.368980205	0.353909135	0.359073197	0.362292941
54,425	C_D	0.023357651	0.022964252	0.023411409	0.02359048
512	C_L	0.3637479	0.35379833	0.357580694	0.360850141
262,144	C_D	0.023084749	0.022706732	0.022902709	0.023082744
1,024	C_L	0.360812844	0.353241712	0.355943711	0.359172468
1,048,576	C_D	0.022934404	0.022593342	0.02270675	0.0228845
2,048	C_L	0.358281928	0.352827907	0.354593186	0.357798948
4,194,304	C_D	0.022799839	0.022534646	0.022606485	0.022782607
continuum	C_L	0.356208937	0.351662793	0.348226045	0.351596613
	C_D	0.022684938	0.02245344	0.02250143	0.022674853

Table 4.2: C_L, C_D of NACA0012 - Vassberg and Jameson [18]

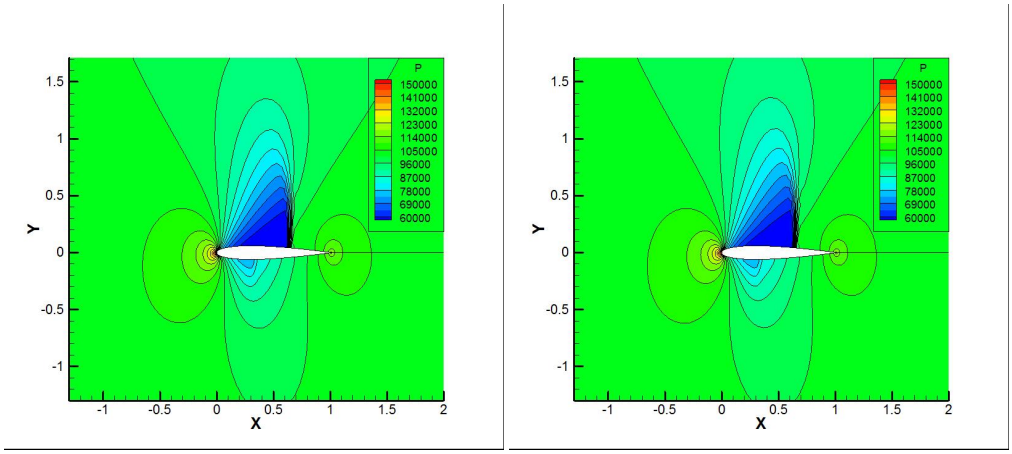

(a) RoeM without scaling

(b) AUSMPW+ without scaling

(c) RoeM with scaling

(d) AUSMPW+ with scaling

Figure 4.1: NACA0012 pressure contours

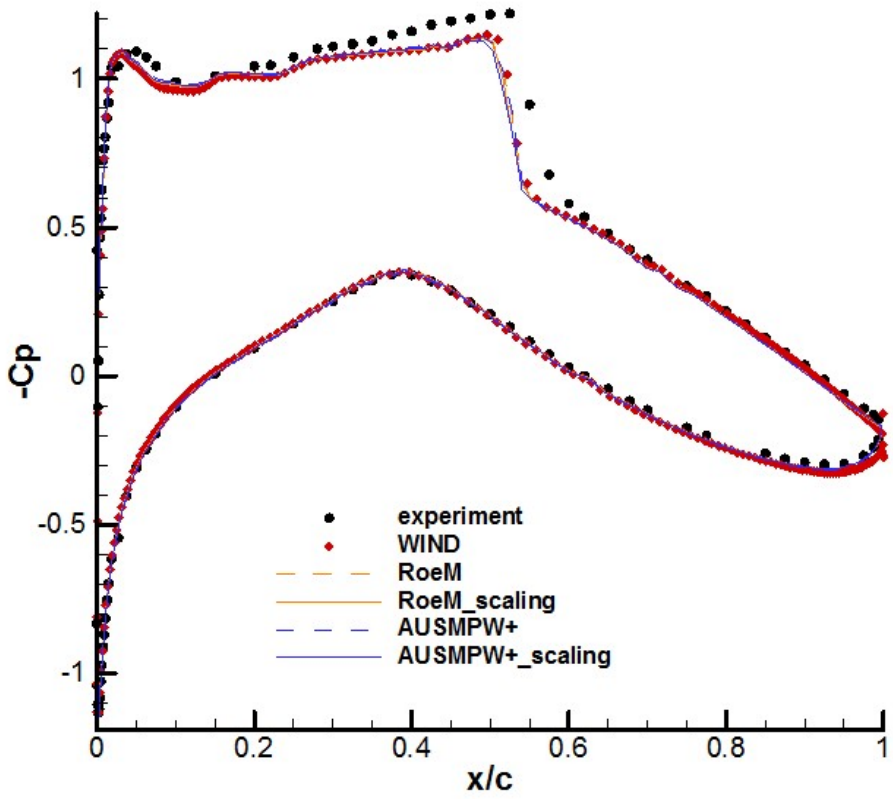

Figure 4.2: C_p curve of RAE2822

4.1.3 Steady Inviscid Flow around a Cylinder

The two-dimensional inviscid flow past a cylinder is a typical low Mach number test case. M_∞ of 0.01 flow is computed with 72x100 O-type grid points and MLP5 is employed. Steady system preconditioning is required due to the low Mach number, and numerical dissipations need to be properly scaled. This problem easily reveals the vulnerability to checkerboard instability of a numerical scheme. Since the preconditioned Roe is known to be completely free from this instability, we choose the preconditioned Roe as a comparison target.

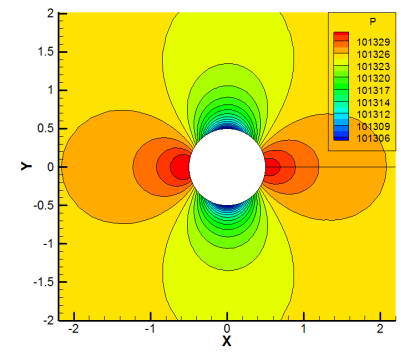

(a) Preconditioned Roe

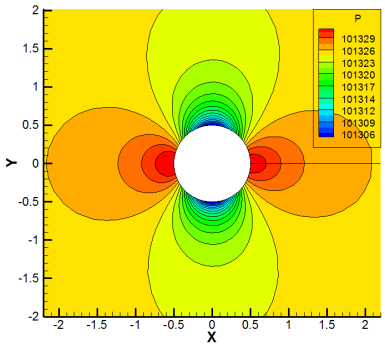

(b) RoeM with scaling

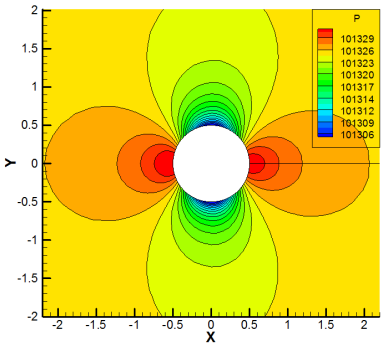

(c) AUSMPW+ with scaling

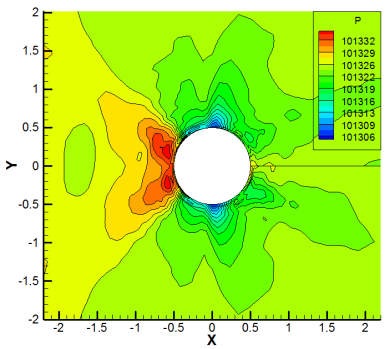

(d) RoeM without scaling

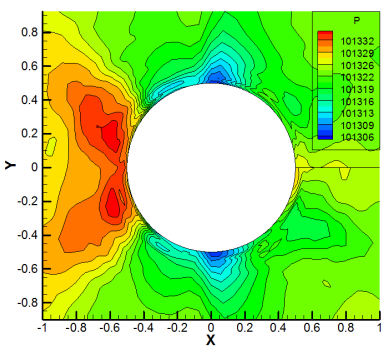

(e) RoeM without scaling-enlarged

Figure 4.3: Pressure contours of the inviscid flow around a cylinder at M_∞=0.01

The results of RoeM and AUSMPW+ with the scaling of numerical dissipations are shown in Figure 4.3 with the result of preconditioned Roe. Three pressure contours agree each other and fully suppress the checkerboard. However, RoeM and AUSMPW+ without proper scaling of numerical dissipations fail to generate satisfactory results. Figure 4.3 (d), (e) represent the defective result with checkerboard instability appeared in RoeM without scaling. We can verify the effects of the scaling of numerical dissipations by this results.

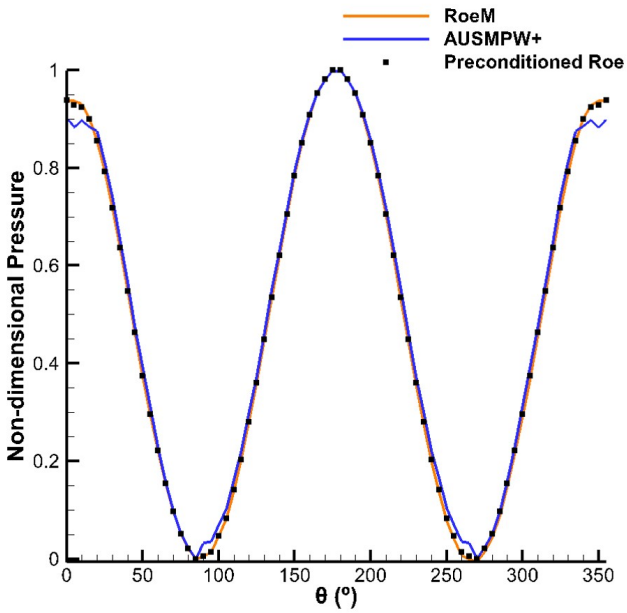

Figure 4.4: Pressure on the cylinder surface at M_∞=0.01

Non-dimensional pressure distribution on the cylinder surface is plotted in Figure 4.4. The results are obtained from properly scaled RoeM and AUSMPW+ with steady system preconditioning. While RoeM and preconditioned Roe show smooth plots, AUSMPW+ has a little dimples in stagnation point around 0° and the maximum speed regions at 90°, 270°.

The abnormality in stagnation point originates from the definition of mean local Mach number in Eq. (3.45). We have followed the mean local Mach number as defined in AUSM+-up [14], but sometimes, the average of right and left Mach numbers is not appropriate as a mean value. We, therefore, redefine this term as follows:

$$\bar{M}^2 = \frac{V_{1/2}^2}{c^2}. \tag{4.1}$$

$V_{1/2}$ is calculated by Roe-average and arithmetic average of right and left velocities. The dimples around 0° disappears when we use Eq. (4.1) with $V_{1/2}$ obtained from both Roe-average and arithmetic average in Figure 4.5. For the legend, 'original' means the use of mean local Mach number of Eq. (3.45), the same definition as AUSM+-up. 'Roe-avg.' and 'arithmetic avg.' mean the use of mean local Mach number of Eq. (4.1). All are calculated by the properly scaled AUSMPW+ scheme with steady preconditioning.

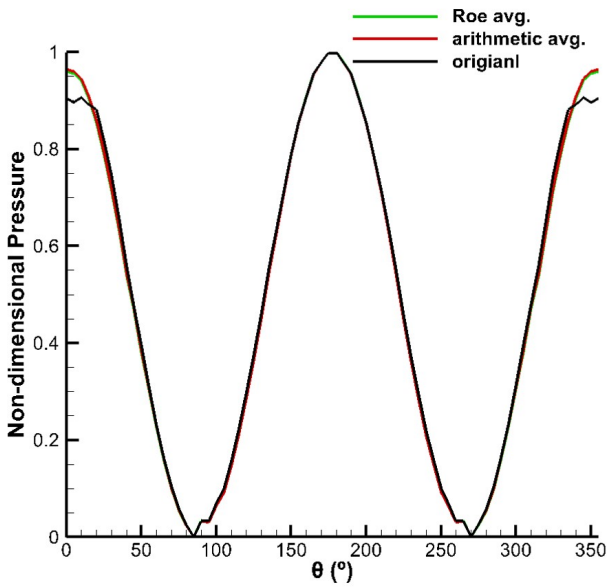

Figure 4.5: Redefined local mean Mach number

The abnormality in the maximum speed regions is, we suppose, ascribed to the process of higher-order interpolation, because the 1st order result of AUSMPW+ does not make such dimples. We changed the interpolation variables from primitive variable **W** to characteristic and conservative variables. Here, the second order MUSCL reconstruction with van Albada limiter is used. Different choice of limiter yields the similar results. As shown in Figure 4.6, the use of primitive and conservative variables for the second order results is fruitless to avoid unwanted dimples around 90° and 270°. However, characteristic variables remove such defect. Again, all plots in Figure 4.6 are computed by the properly scaled AUSMPW+ with steady preconditioning, and the mean local Mach number of Eq. (4.1) with Roe-averaged $V_{1/2}$ is used.

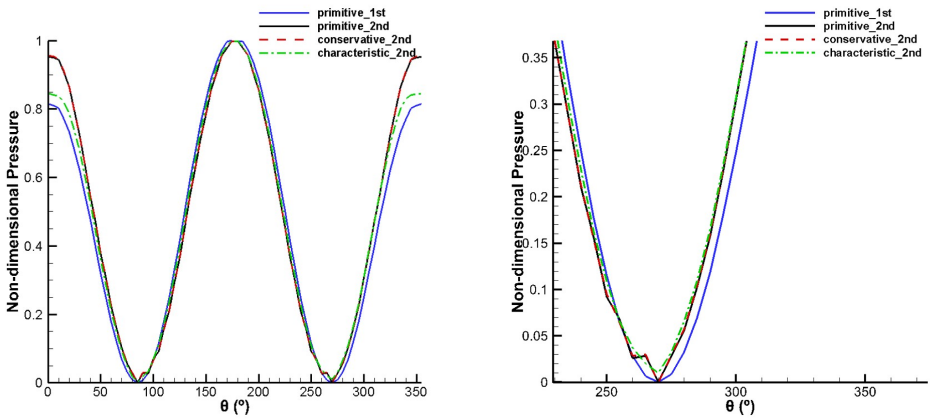

(a) (b) Enlarged view of (a) at 270°

Figure 4.6: Use of different higher-order interpolation variable

4.1.4 Unsteady Inviscid Vortex Propagation

An inviscid propagating vortex is an un steady problem, where some vortex travels at a free stream velocity (U_∞) in time. Ideally, the vortex will maintain

its initial shape with time and simply translate through the domain, but the artificial dissipation in CFD diffuses the vortex. In this study, a simple 2D vortex is used to initialize the domain, and it is assumed that the free stream velocities only exist in the x direction. The velocity distribution is given by

$$\delta u = -U_\infty \beta \frac{y - y_c}{R} e^{-r^2/2}$$
$$\delta v = U_\infty \beta \frac{x - x_c}{R} e^{-r^2/2}$$
$$\delta T = 0.5(U_\infty \beta)^2 e^{-r^2/2}/c_p$$

where

$$u_0 = U_\infty + \delta u, \qquad v_0 = \delta v, \qquad T_0 = T_\infty - \delta T$$
$$\rho_0 = \rho_\infty (\tfrac{T_0}{T_\infty})^{1/\gamma - 1}, \qquad \rho_\infty = \tfrac{p_\infty}{R_{gas} T_\infty}, \qquad p_0 = \rho_0 R_{gas} T_0$$
$$r = \tfrac{\sqrt{(x-x_c)^2 + (y-y_c)^2}}{R}, \qquad U_\infty = M_\infty \sqrt{\gamma R_{gas} T_\infty}.$$

The user defined parameters R, β, and x_c and y_c are the radius, strength, and the starting point of the vortex, respectively. Flow conditions of $M_\infty = 0.005$, $T_\infty = 300K$, $R = 0.03$ and $\beta = 5$ are used with 80x40 grid points and MLP5.

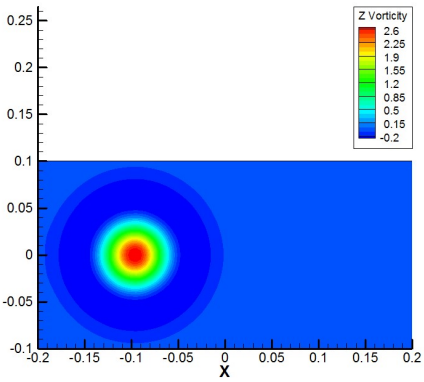

Figure 4.7: Initial contour of vorticity

For the low Mach unsteady problem, unsteady system preconditioning using Strouhal number is essential to enhance the convergence rate within the pseudo-time step. The acoustic speed and the convection speed is used alternately as the velocity scale in the relation of physical $CFL_{\mathcal{U}}$ of Eq. (3.22). Also, the scaling of numerical dissipation is needed for the accuracy in low Mach number limit, hence, we use the properly scaled RoeM and AUSMPW+.

In the case of CFL_V=1, the time step is large enough that the high Strouhal number limit is not reached. Figure 4.8(a) represents the centerline vorticity at some time after the vortex is translated down stream. There is no distinguishable difference between steady and unsteady preconditioners. The properly scaled AUSMPW+ shows a little better accuracy than the properly scaled RoeM. Figure 4.8(b) shows the convergence in the pseudo-time at a given time step. Although steady preconditioner improves convergence from no preconditioning case, unsteady preconditioner outperforms the others. With the moderate value of Strouhal number, we could control the preconditioned sound speed at somewhere between the original sound speed and the local flow speed.

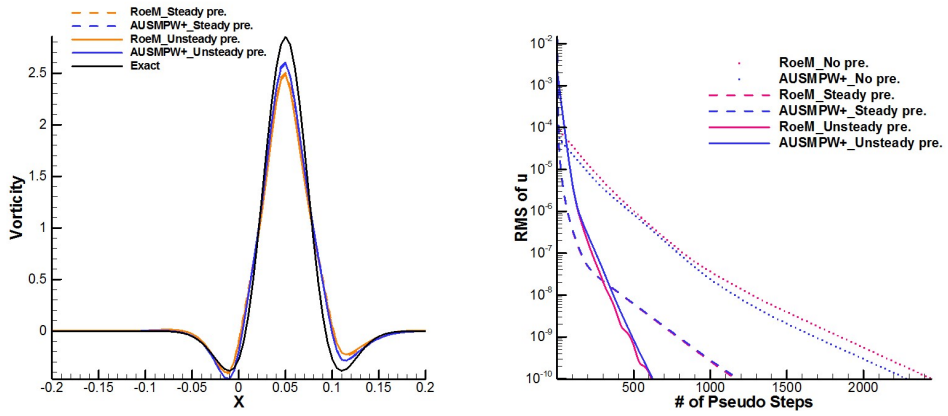

(a) Centerline vorticity at a time step (b) Convergence at a physical time step

Figure 4.8: Plots of propagating vortex with $CFL_V = 1, Str \approx 25.46$

We can examine the high Strouhal number limit with CFL_c=1. Local Str is above 5000, and the unsteady preconditioner makes the system to unpreconditioned time-accurate original system. As you can see in Figure 4.9(b), the convergence at a physical time step shows little difference between no preconditioner case and the unsteady system preconditioner. They show far better convergence that the application of steady preconditioner. For the accuracy, Figure 4.9(a) shows highly accurate results for both steady and unsteady preconditioner, since we treated the scaling of numerical dissipation independently with the preconditioning parameter. From this results, we can confirm that it is important to resolve the acoustic time scale accurately in the high Strouhal limit.

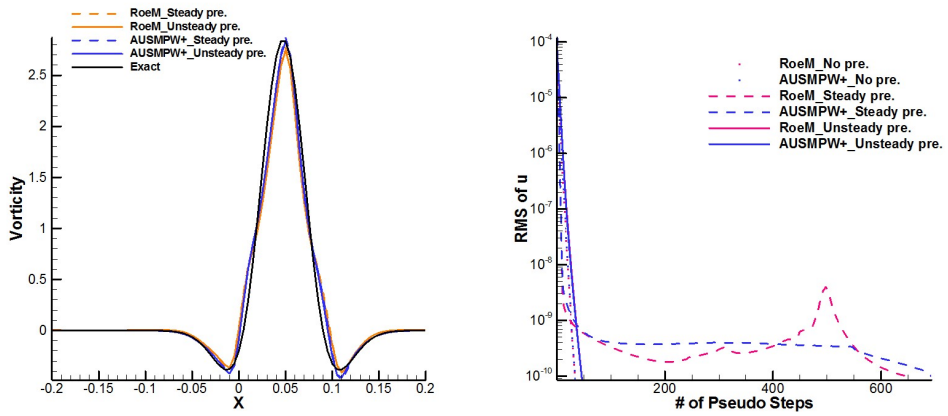

(a) Centerline vorticity at a time step (b) Convergence at a physical time step

Figure 4.9: Plots of propagating vortex with $CFL_c = 1, Str \approx 5092.96$

Previous research on unsteady preconditioning showed the accuracy degradation with matrix diffusion [5], [6] in high Strouhal limit as well as in low Strouhal number flow. They recommended the AUSM-type scheme, because application of unsteady preconditioning to Roe-type scheme sacrifices the ac-

curacy for the convergence in unsteady flow calculations. However, since this study treated the preconditioning and the scaling of numerical dissipation separately, our RoeM result shows excellent accuracy almost equal to the AUSM-type scheme in both low Strouhal number flow and high Strouhal number limit, while the convergence is always best for the unsteady preconditioner.

4.2 Two-phase Flow Computation

4.2.1 Two-phase Shocktube

This problem has been simulated for various AUSM-family schemes [20]. We would like to simulate for properly scaled two-phase RoeM and AUSMPW+. We anticipate the scaling of numerical dissipations does not affect the accuracy in this problem as we verified with transonic airfoils in section 4.1.1 and 4.1.2. Also, newly defined two-phase SDST is tested through this problem. Shock discontinuity and phase interface should be distinguished by $\Pi^{**}_{1/2}$.

Air-to-Water Shocktube

A 1D domain of [0m, 10m] is separated by left and right states at x=5m:

$$(p, \alpha_1, u, T)_L = (10^9 Pa, 1-\epsilon, 100 m/s, 308.15K) \quad \text{for } x \leq 5\text{m, almost air}$$
$$(p, \alpha_1, u, T)_R = (10^5 Pa, \epsilon, 100 m/s, 308.15K) \quad \text{for } x > 5\text{m, almost water}$$

where $\epsilon = 1.0 \times 10^{-7}$. The problem is computed up to 2.0×10^{-3}s with $\Delta t = 2.0 \times 10^{-6}$s, and 500 grid points with $\Delta x = 0.02$m are used. Again, MLP5 is employed. The results of properly scaled two-phase RoeM and AUSMPW+ along with two-phase RoeM and AUSMPW+ without scaling of numerical dissipations are plotted in Figure 4.10. As expected, the four results coincide each other, showing smooth captures of a rarefaction wave ($x \approx 4.5$m), a phase interface ($x \approx 5.5$m), and a shock ($x \approx 8.5$m).

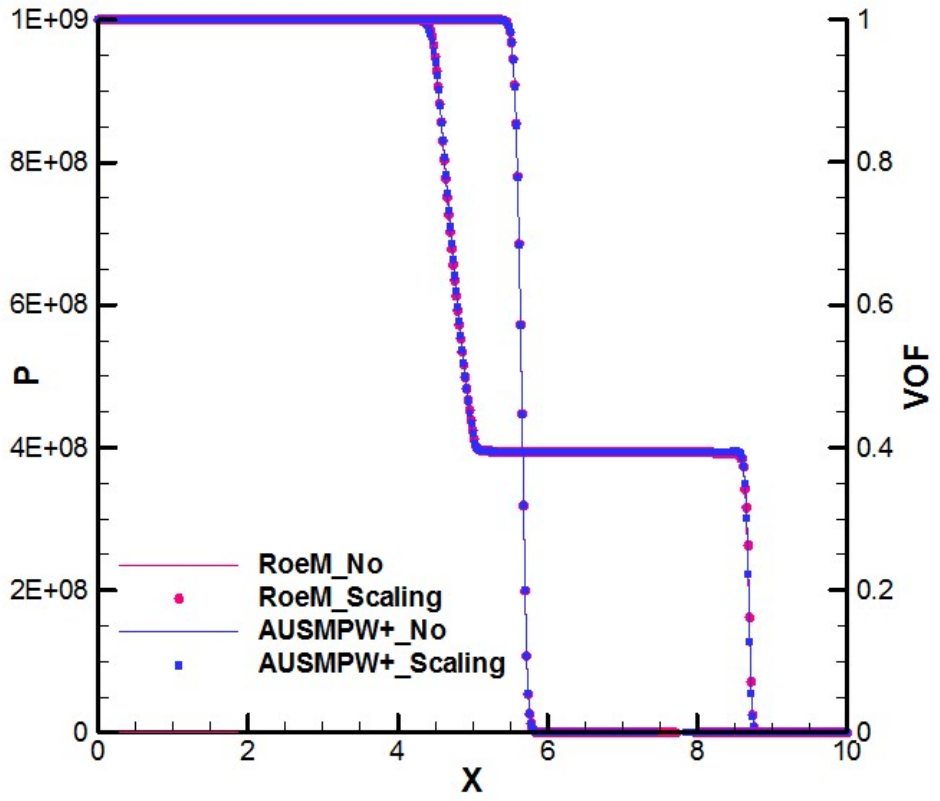

Figure 4.10: Air-to-Water shocktube problem solutions at t=2ms

Water-to-Air Shocktube

A 1D domain of [0m, 10m] is separated by left and right states at x=5m:

$$(p, \alpha_1, u, T)_L = (10^7 Pa, \epsilon, 100 m/s, 308.15K) \qquad \text{for } x \leq 5\text{m, almost water}$$
$$(p, \alpha_1, u, T)_R = (5 \times 10^6 Pa, 1-\epsilon, 100 m/s, 308.15K) \quad \text{for } x > 5\text{m, almost air}$$

where $\epsilon = 1.0 \times 10^{-7}$. The problem is computed up to 2.0×10^{-3}s with $\Delta t = 2.0 \times 10^{-6}$s, and 500 grid points with $\Delta x = 0.02$m are used. Again, MLP5 is employed. Here, again, the four results of properly scaled two-phase RoeM

and AUSMPW+ along with two-phase RoeM and AUSMPW+ without scaling match well. Figure 4.11 shows reasonable capturing of a rarefaction wave ($x \approx$ 2m), a smooth transition at a phase interface ($x \approx$ 5m), and robust shock capturing ($x \approx$ 6m).

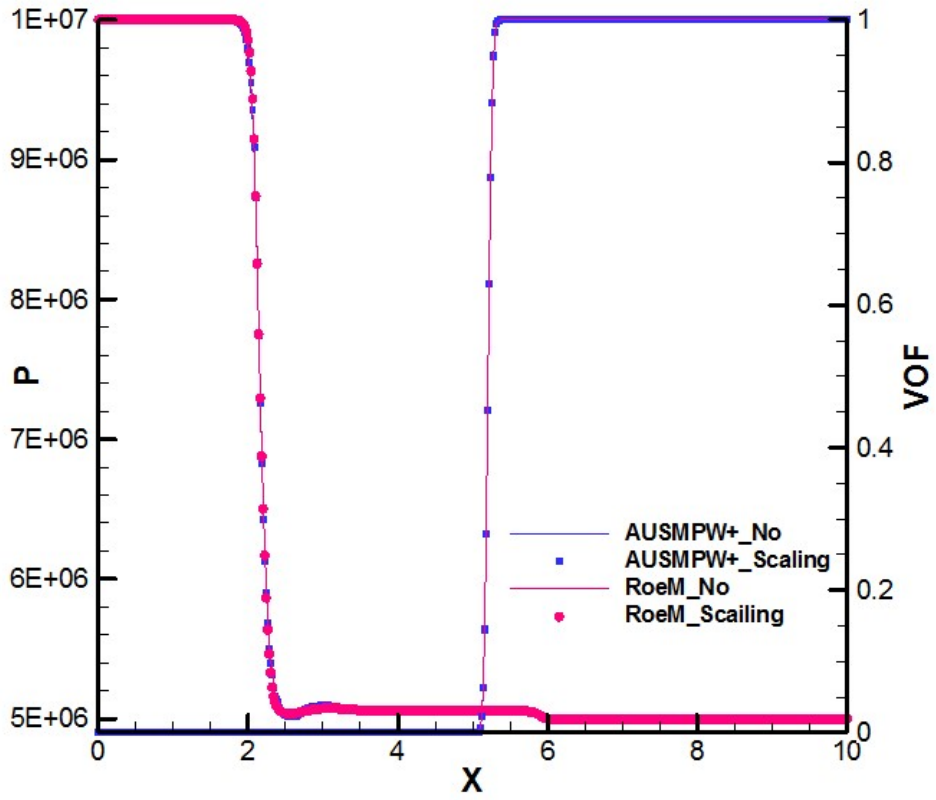

Figure 4.11: Water-to-Air shocktube problem solutions at t=2ms

From these two results, we could verify that the scaling of numerical dissipations employed for the accuracy and stability of low Mach number regions does not affect the accuracy of flows above low Mach limit even for two-phase problems. Also, newly defined SDST proved to sense shock discontinuity only.

4.2.2 Shock/Water-Column Interaction

As a severe benchmark test for compressible two-phase flows, a shock in air impacting on a water-column (i.e., 2D droplet) is simulated. The simulation conditions are as the same as in [20]. 400x200 isotropic cells are used for a domain of [-5mm, 5mm]x[0mm, 5mm] to cover the 6.4mm diameter water-column with its center at origin, i.e., the diameter being 256 times grid spacing $\Delta x_{min} = \Delta y_{min}$=0.025mm in this region; then the cells are stretched toward outer boundaries so that a domain of [-15mm, 20mm]x[0mm, 15mm] is filled with 900x420 cells as a total. The initial conditions are as follows.

$$(p, \alpha_1, u, T)_L = (2.35438 \times 10^5 Pa, 1-\epsilon, 225.86 m/s, 381.85K) \quad \text{for } x \le -4\text{mm}$$
$$(p, \alpha_1, u, T)_R = (1 \times 10^5 Pa, 1-\epsilon, 0 m/s, 293.15K) \quad \text{for } x > -5\text{mm}$$
$$(p, \alpha_1, u, T)_{droplet} = (1 \times 10^5 Pa, \epsilon, 0 m/s, 293.15K) \quad \text{for } x^2 + y^2 < (3.2\text{mm})^2$$

where, $\epsilon = 1.0 \times 10^{-5}$. The shock starts to move with M_{sh}=1.47.

Since the air/water interface having a circular shape should reside on the Cartesian-type grid, we specified a smooth transition region of $\pm 2\Delta x_{min}$ width on the initial phase interface so that the void fraction α_1 is interpolated using the blending function:

$$(\alpha_1)_{adjust} = G(\xi_2)(1-\epsilon) + (1 - G(\xi_2))\epsilon$$
$$G(\xi) = -\xi_2^2(2\xi_2 - 3)$$
$$\xi_2 = \frac{\sqrt{(x^2+y^2)} - (r - 2\Delta x_{min})}{4\Delta x_{min}}, \quad r - 2\Delta x_{min} \le \sqrt{x^2+y^2} \le r + 2\Delta x_{min}.$$

The results with van Leer limiter are shown in Figure 4.12 and 4.13 (in which numerical Schlieren function $(1+\alpha_1^2)\log(|\nabla\rho|+1)$ is used with the range between 4 and 28). Two results of two-phase RoeM and AUSMPW+ are similarly evolved with time. After impacting on the water-column, the shock transmits into the water, while it diffracts as if it moves around a solid object in the air

region. The shock travels faster inside the water-column due to the grater speed of sound. Around 6.75μs, the shock in water is reflected from the rear phase interface (Figure 4.12(c), 4.13(c)), and the reflection occurs repeatedly causing complex flow structures inside the water-column. Here again, two-phase SDST $\Pi^{**}_{1/2}$ effectively senses shock without confusing with circular phase interface.

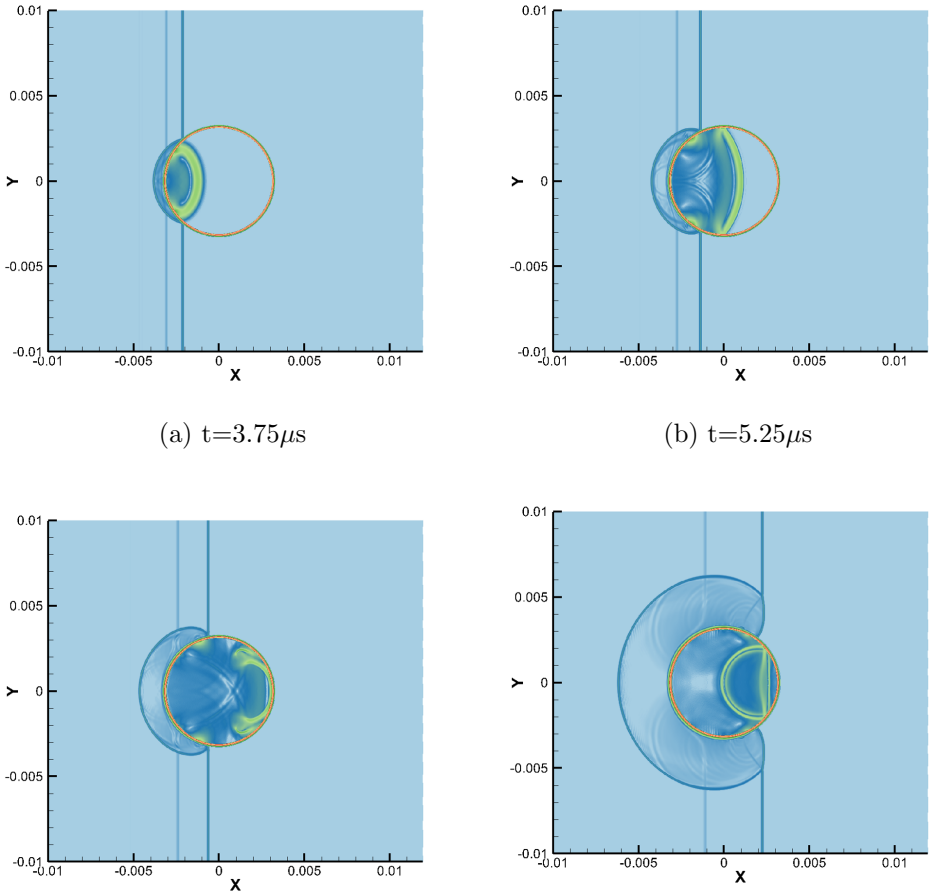

(a) t=3.75μs

(b) t=5.25μs

(c) t=6.75μs

(d) t=12.5μs

Figure 4.12: Time evolution of solution of shock/water-column interaction problem of RoeM

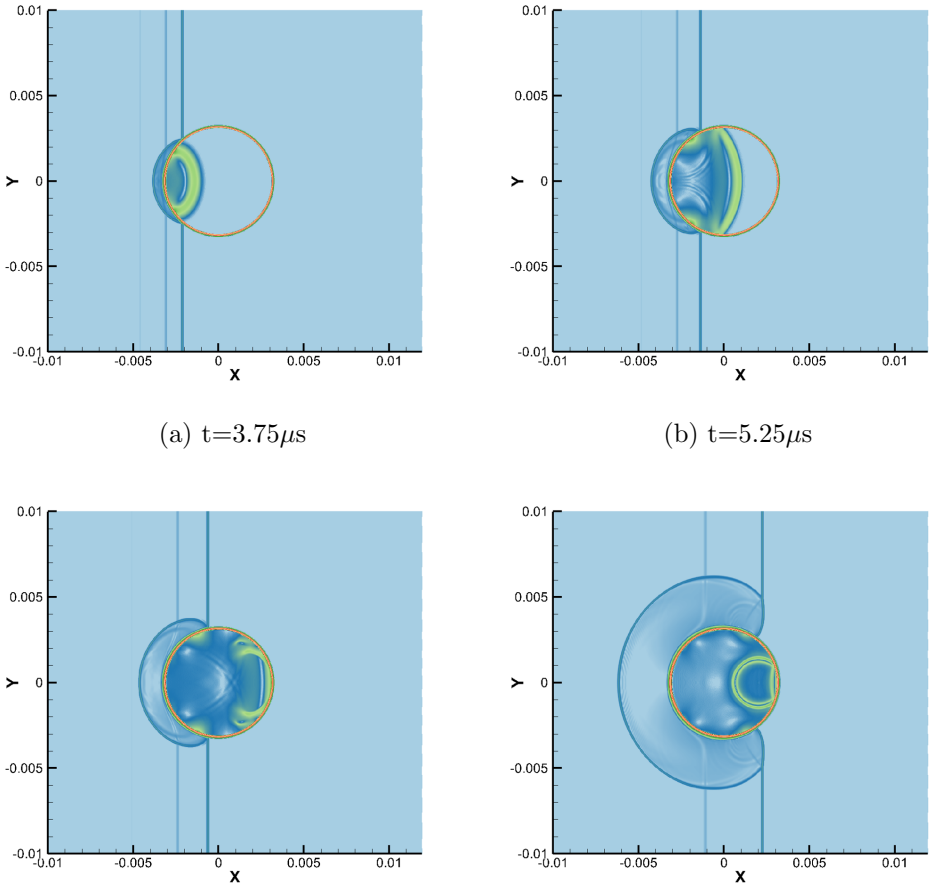

(a) t=3.75μs

(b) t=5.25μs

(c) t=6.75μs

(d) t=12.5μs

Figure 4.13: Time evolution of solution of shock/water-column interaction problem of AUSMPW+

4.2.3 Cryogenic cavitation

Finally, for the validation of the use of general EOS, numerical simulation of experiments by Hord [21] for cryogenic cavitating flow around ogive is presented. Run number 322E case is calculated, where the working fluid is liquid nitrogen, $\sigma_\infty = 0.44,\ U_\infty = 26.8m/s$ and $T_\infty = 88.56K$. Two-phase RoeM with steady preconditioning accompanied by MLP 5th order interpolation is used with total 39,176 mesh points. The employed turbulence model is $k-\omega$ SST, and Kunz's [22], Merkle's [23], Singhal's [24], Mushy IDM [25] cavitation models are used. The regression model based on NIST database [26] is used for the EOS of liquid nitrogen.

Comparisons of pressure and temperature depressions with different cavitation models to the Hord's experiments and Utturkar's calculations [27] are represented in Figure 4.14. A slight difference are observed at the cavitation closure region according to the different cavitation models, but overall, our computational results well match with the reference data (Hord's experiments and Utturkar's calculations). The error in temperature between experiments and calculations are known to be from the thermocouple used in experiments. With these results, we can say that two-phase RoeM and AUSMPW+ with new two-phase SDST $\Pi^{**}_{1/2}$ can compute two-phase flows of any kind of working fluids regardless of the type of EOS.

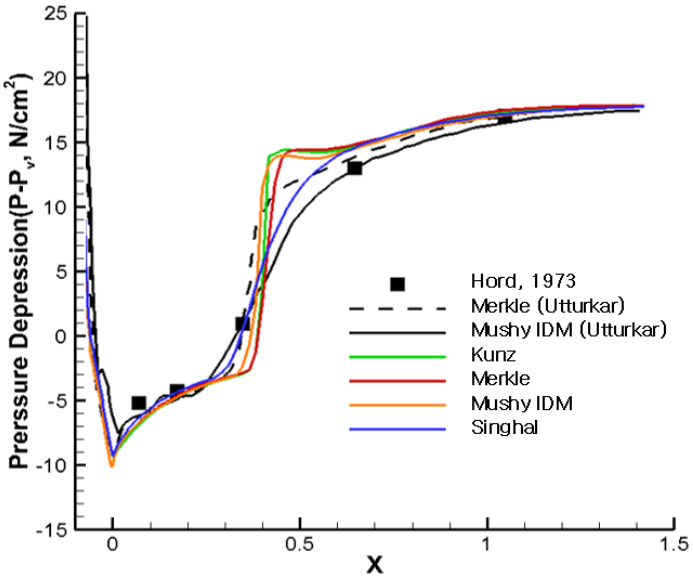

(a) Pressure depression

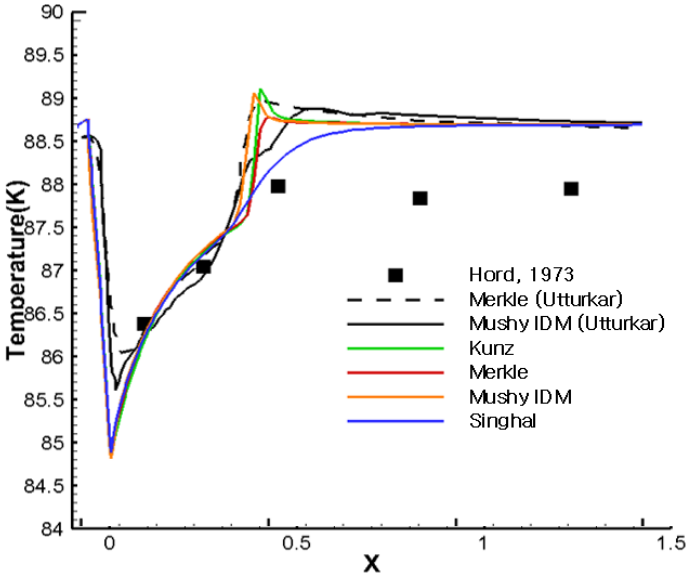

(b) Temperature variation

Figure 4.14: Comparisons of pressure depression and temperature variation with different cavitation models to the experiment's results

Chapter 5

Conclusions

All-speed two-phase RoeM and AUSMPW+ schemes are presented. Many features have been improved compared to previously proposed two-phase RoeM and AUSMPW+.

The first improvement is the extension to the general EOS (equation of state). Although previous two-phase RoeM and AUSMPW+ are efficient and accurate shock-stable schemes, they have a limitation of EOS. The reason for this limitation is that SDST (shock discontinuity sensing term) included in two-phase RoeM and AUSMPW+ is dependent on certain type of EOSs. Since this SDST plays a critical role to impose appropriate amount of dissipations on problematic regions like near shock region, it is important to modify SDST not to be dependent on certain EOSs while maintaining its shock sensing property without confusing with a phase interface. It can be accomplished by new definition of SDST with $\Pi^{**}_{1/2}$ and $\bar{p}^{*}_{L,R}$. They only require the mixture density and the speed of sound at a cell interface which are irrespective of the form of EOS. The performance of newly designed SDST is validated through 1-D shock

relation for various mixture mass fractions. A couple of compressible two-phase simulations proved that the new SDST successfully senses shock discontinuity only without confusing with phase interface, and gives appropriate amount of numerical dissipations to near shock.

The second improvement is the application of unsteady system preconditioning. Since previous two-phase methods have applied only steady preconditioning technique, they could not calculate unsteady flows efficiently and accurately. With the consideration of Strouhal number, this study could achieve unsteady preconditioning. Through vortex propagation problem, it is verified that the unsteady preconditioning remarkably accelerates the convergence rate.

Concerns about preconditioning is its negative effect on the numerical dissipations in low Mach limit. To settle this issue, ideas from an analysis on each term of numerical dissipations are adopted to two-phase RoeM and AUSMPW+. The key is the inclusion or exclusion of global cut-off in the scaling factors. In general, global cut-off is unnecessary in numerator of numerical dissipation, while the terms in denominator should keep the global cut-off. Through this scaling, properly scaled two-phase RoeM and AUSMPW+ are completed. This scaling has no negative effect on the accuracy of moderate or high Mach number regions, but suppresses the instability or accuracy degradation found in low Mach number regions. The suitability of this scaling is confirmed through various compressible or incompressible test cases.

Analysis on unsteady characteristics of cavitation, phase change in nuclear reactor or underwater explosions can be studied further using the product of this study. Until now, reputable research on unsteady cavitation reflecting its compressible nature is almost unprecedented. With unsteady preconditioning and proper scaling of numerical dissipations, it is anticipated that these kind of research will proceed briskly.

Bibliography

[1] H. Kim, D. Min, and C. Kim, "Computations of cryogenic cavitating flow around turbopump inducer," in *Proceedings of ICCFD8*, Chengdu, China, July 2014.

[2] S-W. Ihm and C. Kim, "Computations of homogeneous-equilibrium two-phase flows with accurate and efficient shock-stable schemes," *AIAA Journal*, vol. 46, no. 12, pp. 3012-3037, 2008.

[3] M. A. Potsdam, S. Venkateswaran, and S. A. Pandya, "Unsteady low Mach preconditioning with application to rotorcraft flows," in *Proceedings of the 18th AIAA CFD Conference*, Miami, FL, June 2007.

[4] J. S. Sachdev, A. Hosangadi, and V. Sankaran, "Improved flux formulations for unsteady low Mach number flows," in *42nd AIAA Fluid Dynamics Conference and Exhibit*, New Orleands, LA, June 2012.

[5] A. Hosangadi, J. Sachdev, and V. Sankaran, "Improved flux formulations for unsteady low Mach number flows," in *Proceedings of ICCFD7*, Big Island, Hi, July 2012.

[6] D. Folkner, A. Katz, and V. Sankaran, "An unsteady preconditioning scheme based on Convective-Upwind Split-Pressure (CUSP) artificial dis-

sipation," in *52nd Aerospace Science Meeting*, National Harbor, MD, January 2014.

[7] X-S. Li and C-W. Gu, "Mechanism of Roe-type schemes for all-speed flows and its application," *Computers & Fluids*, vol. 86, pp. 56-70, 2013.

[8] J. M. Weiss and W. A. Smith, "Preconditioning applied to variable and constant density flows," *AIAA Journal*, vol. 33, no. 11, pp. 2050-2056, 1995.

[9] S-s. Kim, C. Kim, O.-H. Rho, and S. K. Hong, "Cures for the shock instability: Development of shock-stable Roe scheme," *Journal of Computational Physics*, vol. 185, pp. 342-374, 2003.

[10] K. H. Kim, C. Kim, and O.-H. Rho, "Methods for the accurate computations of hypersonic flows I. AUSMPW+ scheme," *Journal of Computational Physics*, vol. 174, pp. 38-80, 2001.

[11] H. Luo, J. D. Baum, and R. L"ohner, "Extension of Harten-Lax-van Leer scheme for flows at all speeds," *AIAA Journal*, vol. 43, no. 6, pp. 1160-1166, 2005.

[12] M.-S. Liou, "A sequel to AUSM: AUSM+," *Journal of Computational Physics*, vol. 129, pp. 364-382, 1996.

[13] J. R. Edwards and M.-S. Liou, "Low-diffusion flux-splitting methods for real fluid flows at all speeds," *AIAA Journal*, vol. 38, pp. 1624-1633, 2000.

[14] M.-S. Liou, "A sequel to AUSM, Part II : AUSM+-up for all speeds," *Journal of Computational Physics*, vol. 214, pp. 137-170, 2006.

[15] K. H. Kim and C. Kim, "Accurate, efficient and monotonic numerical methods for multi-dimensional compressible flows: Part II: Multi-dimensional

limiting process," *Journal of Computational Physics*, vol. 208, No. 2, pp. 570-615, 2005.

[16] B. van Leer, "Towards the ultimate conservative difference scheme. V. A. second-order sequel to Godunov's method," *Journal of Computational Physics*, vol. 32, no. 1, pp. 101-136, 1979.

[17] S. Yoon and A. Jameson, "Lower-upper symmetric-Gauss-Seidel method for the Euler and Navier-Stokes equations," *AIAA Journal*, vol. 26, no. 9, 1988.

[18] J. C. Vassberg and A. Jameson, "In pursuit of grid convergence, Part I: Two-dimensional Euler solutions," in *27th AIAA Applied Aerodynamics Conference*, San Antonio, TX, June 2009.

[19] F. R. Menter, "Two-equation eddy-viscosity turbulence models for engineering applications," *AIAA Journal*, vol. 32, no. 8, 1994.

[20] K. Kitamura and M.-S. Liou, "Comparative study of AUSM-family schemes in compressible multiphase flow simulations," in *Proceedings of ICCFD7*, Big Island, Hi, July 2012.

[21] J. Hord, "Cavitation in liquid cryogens III - ogives," National Bureau of Standards, Boulder, CO, Technical Report NASA-CR-2242, 1973.

[22] R. F. Kunz, *et al.*, "A preconditioned Navier-Stokes method for two-phase flows with application to cavitation prediction," *Computers & Fluids*, vol. 29, no. 8, 2000.

[23] C. L. Merkle, J. Z. Feng, and P. E. O. Buelow, "Computational modeling of the dynamics of sheet cavitation," in *Proceedings of 3rd International Symposium on Cavitation*, Grenoble, France, 1998.

[24] A. K. Singhal, *et al.*, "Mathematical basis and validation of the full cavitation model." *Journal of Fluids Engineering*, vol. 124, no. 3, 2002.

[25] I. Senocak and W. Shyy, "Interfacial dynamics-based modelling of turbulent cavitating flows, Part-1: Model development and steady-state computations," *International Journal for Numerical Methods in Fluids*, vol. 44, no. 9, 2004.

[26] NIST Reference Fluid Thermodynamics and Transport Properties Database (REFPROP): Version 8.0, NIST standard Reference Database 23, http://www.nist.gov/srd/nist23.cfm.

[27] Y. Utturkar, "Computational modeling of thermodynamic effects in cryogenic cavitation," Ph. D. Dissertation, Univ. of Florida, 2005.

국문초록

본 연구에서는 기존의 예조건화된 전마하수 이상유동 RoeM과 AUSMPW+ 수치기법을 일반적인 상태방정식과 사용할 수 있도록 확장하고, 비정상 시스템 예조건화 기법과 수치점성 조절을 통하여 더 효율적이고 정확한 전마하수 계산이 가능하도록 하는 연구를 수행하였다. 특정 상태방정식에 종속적인 형태였던 이상유동 RoeM과 AUSMPW+ 기법의 충격파 포착항을 상태방정식에 독립적인 형태로 수정하였고, 새로운 충격파 포착항이 기체상과 액체상의 혼합비에 관계없이 안정적으로 작동하는 것을 확인하였다. 저마하수 비정상 유동 해석을 위하여 Strouhal number를 통하여 비정상 예조건화 기법을 도입하였고, 이를 통해 정상 예조건화 기법을 사용할 때에 비해 수렴속도를 확연히 향상시킬 수 있었다. 또한 시스템 예조건화 파라미터와 수치점성을 조절하는 인자를 독립적으로 취급하여, 수렴성과는 관계없이 저마하수 유동 해석 시의 수치불안정성과 정확성 저하 문제를 해결하였다.

주요어: 전마하수 유동, 이상유동 계산, 예조건화 기법, 수치점성, 충격파 포착항, 일반 상태방정식, 균질 혼합류 모델

학번: 2013-20665